A single-cell transcriptomic atlas reveals resident dendritic-like cells in the zebrafish brain parenchyma

Mireia Rovira[1, 2¶], Giuliano Ferrero[1, 2¶], Magali Miserocchi[1, 2], Alice Montanari[1, 2], Ruben Lattuca[1, 2], Valérie Wittamer[1, 2*]

[1] Institut de Recherche Interdisciplinaire en Biologie Humaine et Moléculaire (IRIBHM), [2] ULB Institute of Neuroscience (UNI), Université Libre de Bruxelles (ULB), Brussels, Belgium

¶ These authors contributed equally to this work

* Author for correspondence: Valerie Wittamer (valerie.wittamer@ulb.be)

KEY WORDS: microglia, macrophages, dendritic cells, zebrafish, *batf3*, *csf1r*, *irf8*

ABSTRACT

Recent studies have highlighted the heterogeneity of the immune cell compartment within the steady-state murine and human CNS. However it is not known whether this diversity is conserved among non mammalian vertebrates, especially in the zebrafish, a model system with increasing translational value. Here, we reveal the complexity of the immune landscape of the adult zebrafish brain. Using single-cell transcriptomics, we characterized these different immune cell subpopulations, including cell types that have not been -or have only been partially- characterized in zebrafish so far. By histology, we found that, despite microglia being the main immune cell type in the parenchyma, the zebrafish brain is also populated by a distinct myeloid population that shares a gene signature with mammalian dendritic cells (DC). Notably, zebrafish DC-like cells rely on *batf3*, a gene essential for the development of conventional DC1 in the mouse. Using specific fluorescent reporter lines that allowed us to reliably discriminate DC-like cells from microglia, we quantified brain myeloid cell defects in commonly used *irf8*$^{-/-}$, *csf1ra*$^{-/-}$ and *csf1rb*$^{-/-}$ mutant fish, revealing previously unappreciated distinct microglia and DC-like phenotypes. Overall, our results suggest a conserved heterogeneity of brain immune cells across vertebrate evolution and also highlights zebrafish-specific brain immunity characteristics.

INTRODUCTION

Over the last years, several landmark studies leveraging high-dimensional techniques have contributed to uncovering the cellular complexity of the human and murine central nervous system (CNS) immune landscapes (Mrdjen et al. 2018; Hammond et al. 2018; Masuda et al. 2019; Van Hove et al. 2019; Jordao et al. 2019; Bottcher et al. 2019). From these works, it was found that, besides parenchymal microglia, the steady-state CNS also harbors diverse leukocytes localized at the CNS-periphery interfaces, including different subtypes of mononuclear phagocytes (MNPs) such as border-associated macrophages (BAMs), monocytes and dendritic cells (DCs)-, along with lymphocytes (T cells, B cells, NK cells or innate lymphoid cells ILCs) and granulocytes (neutrophils). Several of these immune cell populations have since been shown to play important roles in regulating CNS development and homeostasis (Drieu et al. 2022; Pasciuto et al. 2020; Tanabe and Yamashita 2018), or identified as key players in disease models and aging (Alves de Lima et al. 2020; Minhas et al. 2021). Collectively, these studies have highlighted how understanding vertebrate brain leukocyte heterogeneity is key to describe CNS interactions with the microenvironment and other cells such as glial cells, neurons or endothelial cells. By contrast, the repertoire of immune cells in the CNS of other vertebrate models remains less well characterized.

This is the case for the zebrafish, an increasingly recognized model for translational research on human neurological diseases, owing to its robust genetics and conserved physiology with mammals (Turrini et al. 2023; Liu 2023; D'Amora et al. 2023). Zebrafish possess a divers array of immune cells, encompassing both innate and adaptive lineages. Their innate immune compartment includes well-characterized neutrophils and macrophages, which have been extensively studied in both developmental and disease contexts, as well as dendritic cells and monocytes, which remain comparatively less defined (Speirs et al. 2024). In parallel, zebrafish also develop adaptative immune cells such as T and B lymphocytes, which share key molecular and functional features with their mammalian counterparts (Carradice and Lieschke 2008). While immune cells have been described across several organs (Zhou et al. 2023; Wittamer et al. 2011), a comprehensive characterization of the immune cell populations present in the adult zebrafish brain at steady-state is still lacking. This constitutes an essential prerequisite for dissecting the complex cellular orchestration underlying healthy and diseased CNS states. Additionally, although microglia, the CNS-resident macrophages, have been identified in the adult zebrafish brain and profiled using bulk RNA-seq (Oosterhof et al. 2018; Ferrero et al. 2018; Ferrero et al. 2021; Wu et al. 2020), and more recently at single-cell resolution (Zhou et al. 2023; Silva et al. 2021), the extend of phenotypic heterogeneity within the microglial compartment remains unclear. To address this, we established robust protocols for brain dissociation and prospective isolation of leukocytes using fluorescent transgenic lines. By combining this approach with single-cell RNA sequencing, we have generated a gene expression atlas composed of the distinct immune cells present in the homeostatic brain. This dataset revealed the presence of subpopulations of mononuclear phagocytes and other leukocytes, including cell types that have not been -or have only been partially- characterized so far. Here, we present the characterization of a new mononuclear phagocyte population that represents an important fraction among all brain leukocytes and coexist with microglia in the brain parenchyma. This population of cells is *batf3*-dependent and expresses known DC canonical genes. In light of these observations, we have also revisited the phenotype of myeloid-deficient mutant lines, such as *csf1ra*$^{-/-}$, *csf1rb*$^{-/-}$ and *irf8*$^{-/-}$ fish, that have been instrumental to the field. Overall, we provide an overview of the immune landscape in the adult zebrafish brain which, akin to findings in mammals, boasts distinct myeloid and lymphoid cell types.

RESULTS

Mononuclear phagocytes represent the main immune cell population in the adult zebrafish brain

As a first step, we sought to assess the leukocytes present in the zebrafish adult brain according to their cellular morphology. We previously showed the *cd45:DsRe*d transgene labels all leukocytes, with the exception of B lymphocytes (Wittamer et al. 2011; Ferrero et al. 2020). Therefore, we performed May-Grünwald Giemsa (MGG) staining on a pure population of *cd45:DsRed*$^+$ cells isolated from the brain of adult *Tg(cd45:DsRed)* transgenic animals by flow cytometry (**Figure 1A**). Cells with the classical morphological features of mononuclear phagocytes were identified as macrophages/microglia based on their large and vacuolated cytoplasms (**Figure 1B),** in accordance with our previous work (Wittamer et al. 2011). Monocytes, recognized by their kidney-shaped nuclei, were also present, as well as cells with a typical dendritic cell morphology, namely elongated shapes, large dendrites and oval or kidney-shaped nuclei (Lugo-Villarino et al. 2010) (**Figure 1B**). We also found large numbers of lymphocytes, clearly distinguished from myeloid cells by their smaller size and narrow and basophilic cytoplasm stained in blue. The remaining cells were neutrophils, characterized by their clear cytoplasm and highly segmented nuclei.

Next, we took advantage of fluorescent zebrafish transgenic lines, allowing to detect and quantify the different leukocyte subsets using flow cytometry. To achieve this, *Tg(cd45:DsRed)* animals were crossed to established GFP reporters that label mononuclear phagocytes (*Tg(mpeg1:GFP)*), neutrophils (*Tg(mpx:GFP)*, NK and T lymphocytes (*Tg(lck:GFP)*) or IgM-expressing B cells (*Tg(ighm:GFP)*) (**Figure 1A**). For each double transgenic line, we quantified by flow cytometry the proportion of GFP$^+$ cells within the *cd45:DsRed*$^+$ population. As expected, we found that *mpeg1*:GFP$^+$ mononuclear phagocytes were the most abundant leukocytes in the adult brain, accounting for 75.7% ± 2.9 of the total *cd45:DsRed*$^+$ population (n=4) (**Figure 1C,D**). In contrast, *mpx:GFP*$^+$ neutrophils were scarce, representing only 0.2% ± 0.04 of brain leukocytes (n=4) (**Figure 1-supplement 1A**). Regarding lymphocytes, *lck:GFP*$^+$ NK/ T cells were more abundant than *ighm:GFP*$^+$ B cells, accounting for 7.2% ± 0.9 (n=4) and 0.2% ± 0.01 (n=4), respectively (**Figure 1-supplement 1B,C**).

Although *mpeg1*-driven fluorescent transgenes are commonly used to label mononuclear phagocytes, we and others have previously shown that *ighm*-expressing B cells are also marked by these reporters, as they endogenously express *mpeg1.1* (Ferrero et al. 2020; Moyse and Richardson 2020). However, based on the low numbers of brain *ighm:GFP*$^+$ cells identified in our flow cytometry analyses, we estimated their contribution to the *mpeg1*$^+$ population was minimal and that brain *mpeg1*$^+$ cells mostly comprise mononuclear phagocytes. To determine the proportion of microglial cells within the broader population of *mpeg1*$^+$ mononuclear phagocytes, we crossed *Tg(cd45:DsRed)* fish (marking leukocytes), with animals carrying the *Tg(p2ry12:p2ry12-GFP)* transgene (Sieger et al. 2012). P2ry12 is a well-established microglia-specific marker conserved across species, including zebrafish (Mazzolini et al. 2019; Rovira et al. 2022; Ferrero et al. 2018), and has been previously used to distinguish microglia from other brain mononuclear phagocytes (Butovsky et al. 2014). Flow cytometry analysis of brain cell suspensions from double transgenic adults revealed that *p2ry12:GFP*$^+$ microglia accounted for approximately 51% (± 2.9; n=4) of all *cd45:DsRed*$^+$ leukocytes (**Figure 1D,E**). Meanwhile, *mpeg1:GFP*$^+$ represented ~75% of the same *cd45:DsRed*$^+$ population. Since the percentage of *mpeg1:GFP*$^+$*cells exceed that of p2ry12:GFP*$^+$microglia, we inferred that roughly 25% of brain *mpeg1:GFP*$^+$ mononuclear phagocytes lack *p2ry12:GFP* transgene expression and are therefore likely non-microglial in nature. Indeed, based on our cytological observations, this population likely contains a mixture of monocytes and dendritic cells. Collectively, these

119 analyses suggest an important diversity among leukocytes present in the steady-state brain of the adult
120 zebrafish.

121

122 **Single-cell transcriptomics identifies multiple leukocyte populations in the adult brain**

123 To fully characterize the heterogeneity within the zebrafish brain immune landscape, next we turned to
124 single-cell trancriptome profiling. Viable *cd45:DsRed*$^{+}$ cells were FACS-sorted from the steady-state brain
125 of adult *Tg(cd45:DsRed)* animals, then subjected to scRNA-sequencing using the 10X platform (**Figure 2A,**
126 **Appendix 1-Figure 2**). After an unsupervised uniform manifold approximation and projection (UMAP) and
127 single-cell clustering, we obtained a total of 20 cell clusters (**Figure 2B**). A preliminary observation of our
128 dataset, revealed the expression of *cd45* (also known as *ptprc*) in all clusters of the dataset, thus
129 confirming their hematopoietic identity (**Figure 2C**). In addition, expression of canonical genes for
130 mononuclear phagocytes (*mpeg1.1*), neutrophils (*mpx*) or T/ NK cells (*lck*, *lymphocyte-specific protein*
131 *tyrosine kinase*) were found in several clusters (**Figure 2C**). Together, these initial observations indicated
132 that we were able to capture a repertoire of different brain leukocytes represented in individual cluster
133 identities. This is in line with the cell type diversity determined from our cytological and flow cytometry
134 analyses.

135 Cluster annotation was achieved based on expression of defined blood lineage-specific genes previously
136 established in zebrafish (Tang et al. 2017; Hernández 2018; Moore et al. 2016), and from published
137 transcriptomes from human and mouse brain leukocytes (Mrdjen et al. 2018; Jordao et al. 2019;
138 Hammond et al. 2018; Masuda et al. 2019; Van Hove et al. 2019). Using these approaches, we annotated
139 15 clusters. The remaining cells are included in the online material but were not used for further analysis
140 in this study. We identified 7 major leukocyte populations that comprised microglia (MG), macrophages
141 (MF), dendritic-like cells (DC-like), T cells, natural killer cells (NK), innate lymphoid-like cells (ILCs) and
142 neutrophils (Neutro) (**Figure 2B, Table 1**). Expression of the markers for each cluster is visualized plotting
143 the top 50 marker genes (**Figure 2D and Table 2**). Of note, one cluster was annotated as proliferative
144 (Prolif) because of the expression of proliferative markers, suggesting the presence of dividing brain
145 leukocytes, however, marker genes were not indicative of a specific cell type (**Figure 2 B,D and Table 1**).
146 A detailed analysis of the different clusters from the lymphoid and myeloid compartments is presented in
147 the following sections, with an emphasis on microglia and DC-like clusters.

148

149 **The adult zebrafish brain contains innate and adaptive lymphoid cells**

150 Expression of *lck*, a conserved marker for T lymphocytes and NK cells (Moore et al. 2016), identified three
151 clusters of lymphoid cells (**Figure 2C, Table 1**). Two of them expressed T cell-specific marker genes such
152 as *zap70* (tcr-associated protein kinase), TCR co-receptors including *cd4-1*, *cd8a*, *cd8b* and *cd28*, and *il7r*,
153 a cytokine receptor that functions in T cell homeostasis (**Figure 3A,D**), all of them showing conservation
154 between mammals and zebrafish. This suggests that these two *zap70*-expressing clusters contain a mix of
155 CD4^{+} and CD8^{+} T cells, and were thus annotated as Tcells1 and Tcells2. Interestingly, a proportion of cells
156 within these clusters expressed *runx3,* which in mammals has been reported as a regulator of tissue
157 resident memory CD8 T cells in different tissues, including the brain (Milner et al. 2017). The second
158 cluster highly expressed genes previously described as markers for NK cells in the zebrafish whole kidney

159 marrow (WKM) (Tang et al. 2017; Carmona et al. 2017), such as chemokines *ccl36.1* and *ccl38.6*,
160 granzymes *gzm3.2* and *gzm3.3*, *il2rb* and *ifng1* (**Figure 3B,D**). However, expression of novel immune-type
161 receptor (*nitr*) or NK-lysin genes was not detected in brain NK cells, in contrast to WKM NK cells (Carmona
162 et al. 2017; Moore et al. 2016; Yoder et al. 2010). Annotation of these lymphoid clusters was mostly based
163 on a zebrafish WKM reference data set (Tang et al. 2017) and therefore, differences may exist between
164 tissues.

165 Notably, we identified an additional cluster that did not express any of the previously mentioned T cell
166 markers but displayed *il4* and *il13* expression in a large proportion of cells (**Figure 3C,D**). In mammals,
167 these two cytokines identify $CD4^+$ T helper type 2 cells, as well as innate-lymphoid cells type 2 (ILC2s), the
168 innate counterparts of adaptive T helper cells. However, unlike T cells, ILC2s lack antigen receptors and
169 associated co-receptors (Vivier et al. 2018). Interestingly, this cluster was also positive for *gata3*, a
170 transcription factor that regulates the development and functions of ILC2s (Wong et al. 2012). The
171 expression profile identified in this cluster may thus represent the molecular signature of zebrafish ILC2-
172 like cells (Vivier et al. 2016). To test this hypothesis, we performed qPCR analyses on *cd45:DsRed*$^+$ brain
173 cells isolated from *rag2*-deficient fish. We hypothesized that, like their murine counterparts (Spits and
174 Cupedo 2012), *rag2* mutant zebrafish, which lack T and B cells (Tang et al. 2014), would still produce ILC-
175 like cells. Supporting this postulate, while the expression levels of *lck* and *zap70* was significantly reduced
176 in brain leukocytes from the *rag2* mutants in comparison with that from their *wild-type* siblings (**Figure**
177 **3E**), *gata3*, *il4* and *il13* showed similar expression levels between cells from both genotypes (**Figure 3E**). It
178 thus appears that the expression of putative ILC2 cell-associated genes in brain leukocytes is not changed
179 in the absence of T cells. Altogether, these findings support our annotation of this cluster as ILC-like cells.

180

181 **Cellular diversity of the mononuclear phagocyte system in the adult zebrafish brain**

182 As shown in **Figure 2C**, expression of *mpeg1.1*, a canonical marker for mononuclear phagocytes, was
183 identified in nine clusters of our dataset. Four clusters were annotated as microglia (MG), one as
184 macrophages (MF) and four as dendritic-like cells (DC-like) (**Figure 2B and Table 1**).

185 MG clusters (MG1, MG2, MG3, MG4) differentially expressed zebrafish microglial genes such as the
186 lipoproteins *apoc1* and *apoeb* (Herbomel, Thisse, and Thisse 2001; Peri and Nusslein-Volhard 2008;
187 Ferrero et al. 2018; Mazzolini et al. 2019), *ms4a17a.10* (Oosterhof et al. 2018) - a member of the
188 membrane-spanning 4A gene family-, galectin 3 binding protein *lgals3bpb* (Rovira et al. 2022; Kuil et al.
189 2019), and hepatitis A virus cellular receptors *havcr1* and *havcr2* (Kuil et al. 2019; Oosterhof et al. 2018)
190 (**Figure 4A,D**). Moreover, *csf1ra* and *csf1rb,* the zebrafish paralogs of CSF1R and well conserved regulators
191 of microglia development and homeostasis (Oosterhof et al. 2018; Ferrero et al. 2021; Hason et al. 2022),
192 were also identified as marker genes, although their level of expression differed between microglia
193 clusters (**Figure 4D, Table 1**). Importantly, expression of canonical microglial genes were also found in the
194 MG clusters such as *p2ry12*, *hexb*, *mertka* and members of the *c1q* genes, among others, supporting a
195 conserved microglial phenotype (Butovsky et al. 2014; Jurga, Paleczna, and Kuter 2020; Butovsky and
196 Weiner 2018; Gerrits et al. 2020) (**Figure 4-supplement 1**).

197 We also found a cluster of *mpeg1.1*-expressing cells that we annotated as *non-microglia macrophages*
198 (MF). Similar to the microglia clusters (MG), this cluster differentially expressed macrophage-related
199 genes such as *marco*, *mfap4, csf1ra* and components of the complement system (e.g. *c1qb*) (**Figure 4B,D,**

Table 1). However, this cluster differed from the four microglia clusters because microglia markers were not found. This cluster also showed high expression of calcium binding proteins such as *s100a10b*, *anxa5b* and *icn,* as well as the coagulation factor XIII *f13a1b*, among others (**Figure 4B,D and Table 1**). In contrast to mammals, the distinction between microglia and other macrophages in the adult zebrafish brain (i.e. border-associated macrophages) is still unclear (Silva et al. 2021) and to date, no known marker or fluorescent reporter line is available to distinguish these two related cell types. Another possibility is that these *mpeg1.1*-expressing cells are blood-derived monocytes/macrophages. In order to better characterize these two *mpeg1.1*-expressing clusters we performed a differential expression analysis between MF and MG (all four clusters together). As shown in **Figure 4E**, microglial genes such as *apoeb*, *apoc1*, *lgals3bpb*, *ccl34b.1*, *havcr1* and *csf1rb* were significantly down-regulated, whereas macrophage-related genes such as *s100a10b*, *sftpbb*, *icn*, *fthl27*, *anxa5b*, *f13a1b* and *spi1b* were significantly up-regulated (**Table 3**). Therefore, these genes may thus serve as novel markers to discriminate these two related types of macrophages.

Finally, our analysis identified a third group of *mpeg1.1*-expressing cells represented in four clusters (DC1, DC2, DC3, DC4) (**Figure 2B**). Highly expressed genes in these clusters included *siglec15l* (sialic acid binding Ig-like lectin 15, like) and *ccl19a.1* (C-C motif ligand 19a), a putative ligand of the zebrafish T cell receptor *ccr7* (Wu et al. 2012) (**Figure 4C,D and Table 1**). Intriguingly, these four clusters expressed *id2a*, *xcr1a.1*, *batf3* (*basic leucine zipper ATF-like 3 transcription factor*), and *flt3* (**Figure 4C,D and Table 1**), which are the orthologs of the mammalian Id2a, Xcr1, Batf3 and Flt3 genes, required for development and/or functions of conventional dendritic cells (cDC1) (Cabeza-Cabrerizo et al. 2021). These clusters also expressed *chl1a* (adhesion molecule L1), reported to promote DC migration through endothelial cells (Maddaluno et al. 2009) and *hepacam2* (**Figure 4D, Table 1**), frequently found in mammalian DC expression datasets. However, all four clusters had negligible expression of any of the microglia or macrophage markers previously mentioned (**Figure 4D, Table 1**). Based on their transcription profile and possible shared characteristics with mammalian DCs, these clusters were annoted as DC-like cells (DC1, DC2, DC3, DC4).

We next conducted a differential expression analysis of DC-like cells (DC1, DC2, DC3, DC4) versus MG (MG1, MG2, MG3, MG4), as two separate clusters. As shown in **Figure 4F**, significantly different genes include genes previously found as DC-like (up-regulated) or microglial (down-regulated) markers, thus confirming their distinct transcriptomic profiles. In addition DC-like cells could also be identified based on differential expression of *irf8*, *ptprc* and *mpeg1.1*, all significantly up-regulated in this population in comparison to MG (**Figure 4F, Table 3**). This is similar to mammalian cDC1, which are IRF8^{high}, PTPRC(CD45)^{high} and MPEG1^{high} (Cabeza-Cabrerizo et al. 2021), and thus strenghtens the idea that DC-like cells phenotypically resemble mammalian cDC1. In order to explore the biological function of MG and DC-like cells, we performed pathway enrichment analysis (using GO Biological Processes and Reactome) for each MG and DC-like markers (**Table 4 and see Materials and Methods**). This analysis enriched for terms in MG such as *endosomal lumen acidification* (e.g. H+ ATPase family genes), *synapse pruning* (e.g. C1QC/*c1qc*), *response to lipoprotein particle* (e.g. ABCA1/*abca1b*, APOE/*apoeb*), *interleukin-10 signalling* (e.g. IL10RA/*il10ra*), *macrophage activation* (e.g. CTSC/*ctsc*, HAVCR2/havcr2), *MHC class II antigen presentation* (e.g. CD74/*cd74a*, HLA-DOB/mhc2b), *complement cascade* (e.g. C1QA/*c1qa*, CFP/cfp), *mononuclear cell migration* (e.g. CSF1R/*csf1rb*, CMKLR1/*cmklr1*) or *phagocytosis* (e.g. MERTK/*merkta*, MARCO/*marco*) (**Figure 4 supplement 2A, Table 4 and see Materials and Methods**). Enriched terms in DC-like included *FLT3 signaling* (e.g. FLT3/flt3), *myeloid cell differentiation* (e.g. BATF3/batf3, ID2/*id2a*),

243 *Rac2 GTPase cycle* (e.g. RAC2/*rac2*, CDC42/*cdc42l*), *Fc receptor signaling pathway* (e.g. FCER1G/*fcer1g*),
244 *cell chemotaxis* (e.g. CCL19/*ccl19a.1*, XCR1/*xcr1a.1*), innate signaling pathways such as *toll-like receptor*
245 *cascades* (e.g. TLR6/*tlr1*, IRAK3/*irak3*) as well as terms involved in adaptive immunity such as *alpha-beta*
246 *T cell activation* (e.g. CBLB/*cblb*, SOCS1/*socs1*) or *lymphocyte activation involved in immune response* (e.g.
247 *IL12B/il12ba*) (**Figure 4-supplement 2B**). Moreover, we used the Enrichr tool to predict the annotation of
248 the MG and DC-like clusters using the PanglaoDB database that contains multiple single-cell RNA
249 sequencing experiments from mouse and human (Franzen, Gan, and Bjorkegren 2019). The three top
250 significant cell types for MG marker genes were "microglia", "monocytes" and "macrophages" while for
251 DC-like were "Dendritic Cells", "Plasmacytoid DCs" and "Langerhans Cells" (**Figure 4-supplement 2C,D**).

252

253 **Two phenotypically distinct populations of mpeg1$^+$ cells within the brain parenchyma**

254 Having demonstrated the diversity of the immune landscape of the adult zebrafish brain, we next sought
255 to investigate the tissue localization of the different leukocyte populations identified in our dataset, using
256 the same transgenic lines as in **Figure 1**. To differentiate microglia from the two phenotypically distinct
257 populations of brain mononuclear phagocytes (MF and DC-like), we first examined adult brain sections of
258 *Tg(mpeg1:GFP)* and *Tg(p2ry12::p2ry12-GFP)* single transgenic fish immunolabeled for GFP and the pan-
259 leukocytic marker L-plastin (Lcp1). We found the majority of L-plastin$^+$ cells within the brain parenchyma
260 co-expressed the *mpeg1:GFP* transgene (**Figure 5A-C**). Upon examination of *Tg(p2ry12:p2ry12-GFP)* fish,
261 however, we observed that not all parenchymal L-plastin$^+$ cells were GFP (**Figure 5D-F**). Analysis of
262 *Tg(p2ry12:p2ry12-GFP; mpeg1:mCherry)* double transgenics confirmed these observations, a.k.a that a
263 fraction of *mpeg1:mCherry$^+$* cells was negative for the microglial *p2ry12:p2ry12-GFP* transgene (**Figure 5G-**
264 **J**). This suggested that non-microglia mpeg1-expressing cells are present in the brain parenchyma.
265 Interestingly, in contrast to GFP$^+$; mCherry$^+$ microglia which are abundant across brain regions, GFP$^-$;
266 mCherry$^+$ cells particularly localized in the ventral part of the posterior brain (midbrain and hindbrain)
267 (**Figure 5G-J**). Notably, these cells presented with a highly branched morphology when compared to GFP$^+$;
268 mCherry$^+$ microglia.

269 Based on these findings, we next investigated brain samples from *Tg(mhc2dab:GFP; cd45:DsRed)* fish,
270 where co-expression of both fluorescent reporters specifically labels mononuclear phagocytes (Wittamer
271 et al. 2011; Ferrero et al. 2018). In our previous work, we had already observed that, in the brain of these
272 animals, two phenotypically distinct cell populations could be isolated by flow cytometry based on
273 differential *cd45:DsRed* expression levels. While the *cd45^{low}*; *mhc2$^+$* fraction was clearly identified as
274 microglia due to their specific expression of *apoeb* and *p2ry12*, the exact identity of the *cd45^{high}*; *mhc2$^+$*
275 cells remained unclear. However, we initially found these cells lack expression of *csf1ra* transcripts
276 (Ferrero et al. 2018) which, in light of our single cell transcriptomic data, excluded them as macrophages
277 and point to a DC-like cell identity. So, to evaluate the tissue localization of *cd45^{high}; mhc2$^+$* cells, we
278 performed direct imaging of transgene fluorescence on vibratome brain sections from *Tg(mhc2dab:GFP;*
279 *cd45:DsRed)* fish (**Figure 5K**). Most GFP$^+$ cells were DsRed negative, suggesting the low expression of the
280 *cd45* transgene in microglia likely precluded direct imaging of DsRed in these cells. However, in the ventral
281 part of the posterior brain (midbrain and hindbrain), we observed a clear population of GFP$^+$; DsRed$^+$ cells,
282 with a highly ramified morphology (**Figure 5K-N, Figure 5-supplement 1**). The reliable detection of
283 endogeneous DsRed signal in these cells likely identified them as DsRed^{high}. Altogether, these observations
284 strongly suggested that the *mpeg1$^+$; p2ry12$^-$* and *cd45^{high}; mhc2$^+$* cells represent the same parenchymal,

non microglial population, possibly corresponding to the putative DC-like cells identified in our single-cell transcriptomic dataset.

Finally, we also examined the localization of neutrophils and lymphoid cells, labeled using the *Tg(mpx:GFP)*, *Tg(lck:GFP)* and *Tg(ighm:GFP)* lines, respectively (**Figure 5-supplement 1**). In accordance with *mpeg1*$^{+}$*; Lcp1*$^{+}$ cells being the main leukocyte population present in the adult zebrafish brain parenchyma and with our previous flow cytometry analysis, *mpx*$^{+}$, *lck*$^{+}$ and *ighm*$^{+}$ cells were rarely found and, if present, they were located at the border of the sections or lining the ventricles (**Figure 5-supplement 1**).

Collectively, our findings demonstrated that the adult zebrafish brain parenchyma contains at least two phenotypically distinct populations of mononuclear phagocytes: microglia, and a population of highly branched cells with restricted spatial distribution. Notably, these two populations can be reliably distinguished using a combination of existing transgenic lines.

Transcriptomic analyses identify DC-like cells as a parenchymal population along with microglia

To assess whether brain *mpeg1:mCherry*$^{+}$*; p2ry12:GFP*$^{-}$ and *cd45:DsRed*^{high}*; mhc2:GFP*$^{+}$ cells do indeed represent a population distinct from microglia, we next performed bulk transcriptomic analyses to compare their expression profiles. As a source for these studies, we used both *Tg(p2ry12::p2ry12-GFP; cd45:DsRed)* and *Tg(mhc2dab:GFP; cd45:DsRed)* adult fish, allowing to FACS-sort microglia identified in these animals as GFP^{+}; DsRed^{+} or GFP^{+}; DsRed^{low} cells, respectively (Ferrero et al. 2018). The second population of interest was obtained using the *Tg(mhc2dab:GFP; cd45:DsRed)* reporter, and isolated as GFP^{+}; DsRed^{high} cells (**Figure 6A-C**).

Differential expression analysis between *mhc2dab:GFP*$^{+}$*; cd45:DsRed*^{high} (or putative DC-like cells) and *p2ry12:GFP*$^{+}$*; cd45:DsRed*$^{+}$ (or microglia) cells showed up-regulation of DC-like genes previously found in our single-cell transcriptomic analysis (**Figure 6D, Table 5**). Similar results were obtained when comparing DC-like cells with microglia FACS-sorted as *mhcdab*$^{+}$; *cd45*$^{+}$ cells (**Figure 6E, Table 5**). These analyses confirm that our annotated DC-like cluster and *cd45:DsRed*^{high}*; mhc2dab:GFP*$^{+}$ cells share a similar transcriptome distinct from microglia.

Interestingly, a previous study reported the presence of two heterogenous populations of *mpeg1*-expressing cells in the adult zebrafish brain. These cells, which were annotated as *phagocytic* and *regulatory* microglia, could be discriminated based on differential expression of the *ccl34b.1:GFP* reporter (Wu et al. 2020). Interestingly, these two populations displayed a similar morphology, neuroanatomical location and differential gene expression pattern than the annotated DC-like and microglia populations identified in our dataset. We thus re-analyzed the data from Wu et al.. Differential expression between *regulatory* (*ccl34b.1*$^{-}$; *mpeg1*$^{+}$) and *phagocytic* (*ccl34b.1*$^{+}$; *mpeg1*$^{+}$) cells demonstrated up-regulation of genes such as *siglec15l*, *spock3*, *chl1a*, *flt3*, *hepacam2*, *ccl19a.1*, *id2a* and *epdl1*, and down-regulation of genes such as *p2ry12*, *ccl34b.1*, *apoeb*, *apoc1*, *lgals3bpb*, *lgals9l1* and *havcr1*, among others (**Figure 6-supplement 1A and Table 5**). Notably, a large proportion of these DE genes overlapped with that previously found when comparing *mhc2dab:GFP*$^{+}$*; cd45:DsRed*^{high} DC-like cells and *p2ry12:GFP*$^{+}$*; cd45:DsRed*$^{+}$ microglia (**Figure 6-supplement 1B,C and Table 5**). B cell-related genes such as *ighz* and *pax* were up-regulated (**Figure 6-supplement 1A**), suggesting the presence of B cells in the *ccl34b.1*$^{-}$; *mpeg1*$^{+}$

fraction, as expected (Ferrero et al. 2020; Moyse and Richardson 2020). In addition, the expression profile of *ccl34b.1*$^{+}$; *mpeg1*$^{+}$ *phagocytic* microglia strongly correlated with that of *p2ry12:GFP*$^{+}$*; cd45:DsRed*$^{+}$ and *mhc2dab:GFP*$^{+}$; *cd45:DsRed*$^{+}$ microglia (0.76 and 0.71, respectively), whereas *ccl34b.1*$^{-}$; *mpeg1*$^{+}$ *regulatory* microglia correlated with *mhc2dab:GFP*$^{+;}$ *cd45:DsRed*^{high} DC-like cells (0.57) (**Figure 6-supplement 1D,E and Table 5**). Collectively, these findings suggest that, at the transcriptomic level, *ccl34b.1*$^{+}$*; mpeg1.1*$^{+}$ cells correspond to microglia in our dataset, and *ccl34b.1*; $^{-}$*mpeg1*$^{+}$ cells resemble the population we annotated as DC-like cells.

Brain parenchymal DC-like cells are *batf3*-dependent

Our results so far suggested the existence of a putative DC-like cell population located in the parenchyma of the healthy zebrafish brain. To strenghten our findings, we next developed a strategy to assess the identity of this population. We reasoned that the development of the zebrafish counterparts of mammalian cDC1 would likely rely on a conserved genetic program. In our single-cell transcriptomic analysis, zebrafish DC-like cells expressed *batf3*, a cDC1-required transcription factor in human and mouse (Cabeza-Cabrerizo et al. 2021). Therefore, using CRISPR/Cas9 technology we generated a zebrafish *batf3* mutant as a model to explore the lineage identity of putative zebrafish DC-like cells. This mutant line carries a 8-bp deletion downstream of the ATG start, leading to a frameshift mutation and the generation of three premature stop codons (**Appendix 2-Figure 7**). The resulting protein lacks the DNA binding and basic-leucine zipper domains and is likely to be non-functional. To evaluate whether brain DC-like cells were present in these animals, we crossed the *batf3* mutant line to *Tg(p2ry12:p2ry12-GFP; mpeg1:mCherry)* double transgenic fish, and performed immunostainings of adult brain sections (**Figure 7A-J**). Because DC-like cells are abundant in the ventral posterior brain, we quantified the dorsal (mostly containing the optic tectum) and ventral areas separately, as well as the whole section. The numbers of GFP^{+}; mCherry^{+} ; Lcp1^{+} microglia were similar to their *wild-type* siblings, whereas the ventral posterior brain of homozygous *batf3* mutants was largely devoid of GFP^{-}; mCherry^{+}; Lcp1^{+} cells, which identify DC-like cells in our model (**Figure 7K-M**). Moreover, we did not observe any changes in the density of other brain leukocytes (**Figure 7-supplement 1A-C**). Flow cytometry analyses of brain cell suspensions confirmed the dramatic loss of GFP^{-}; mCherry^{+} cells in the absence of *batf3* (2.98% ± 0.588, n=6 versus 0.77 ± 0.097, n=10) (**Figure 7 N,O**). Notably, expression of DC-like markers was barely detectable in the remaining GFP^{-}; mCherry^{+} cells (**Figure 7-supplement 1D,E**). However, these cells also displayed lower mCherry signal intensity, suggesting they most likely represent non-parenchymal *mpeg1*-expressing MF or B cells (**Figure 7-supplement 1F,G**). Regarding GFP^{+}; mCherry^{+} microglia, their proportion was unchanged when compared to that of control fish (**Figure 7 N,O**), which is concordant with our initial observations. Finally, we also performed direct imaging of transgene fluorescence on vibratome brain sections of *batf3* mutants carrying the *cd45:DsRed* transgene. In line with our observations, we found that loss-of-function of *batf3* in *Tg(cd45:DsRed)* transgenic fish resulted in the complete absence of DsRed^{high} DC-like cells in the ventral area of the midbrain parenchyma in comparison with control brains (**Figure 7-supplement 1H-K**). Collectively, these results demonstrated that, the population we annotated as DC-like cells is *batf3*-dependent similar to mammalian cDC1. These results reinforced our hypothesis that these cells represent the zebrafish counterparts of mammalian cDC1.

Characterization of microglia and dendritic-like cells in mononuclear phagocyte-deficient mutants.

367 The presence of two distinct mononuclear phagocyte subsets in the brain parenchyma made us wondered
368 about their respective status in commonly used microglia-deficient zebrafish lines, as they were all initially
369 characterized using the pan-mononuclear phagocyte *Tg(mpeg1:GFP)* reporter (Oosterhof et al. 2018;
370 Ferrero et al. 2021; Wu et al. 2020). With the ability to discriminate between both populations of microglia
371 and DC-like cells, we thus next sought to examine in more details the phenotype of the *irf8*$^{-/-}$, *csf1ra*$^{-/-}$,
372 *csf1rb*$^{-/-}$ and *csf1ra*$^{-/-}$; *csf1rb*$^{-/-}$ double mutant (*csf1r*^{DM}) alleles. To do so, we crossed each mutant line to
373 *Tg(p2ry12:p2ry12-GFP)* animals and analyzed brain sections costained for GFP and L-plastin (**Figure 8**).
374 According to our model, in this setup microglia will be labeled as GFP^{+}; Lcp1^{+}, while GFP^{-}; Lcp1^{+} cells will
375 mostly include DC-like cells, easily identified based on their typical ramified cell shape (**Figure 8A-D**). In
376 addition to DC-like cells, GFP^{-}; Lcp1^{+} cells may also include lymphocytes and/or neutrophils, which are
377 anyway in much lower numbers than mononuclear phagocytes in the adult brain (**Figure 1D**).

378 IRF8 is a transcription factor essential for the development of mononuclear phagocytes in vertebrates
379 (Yanez and Goodridge 2016), including zebrafish (Ferrero et al. 2020), where absence of *irf8* results in lack
380 of microglia (Shiau et al. 2015; Earley, Graves, and Shiau 2018). In line with these findings, we found that
381 adult *irf8* homozygous displayed a dramatic, albeit not complete, reduction of GFP^{+} microglial cells (**Figure**
382 **8E-H, U,W**). Interestingly, most remaining microglia localized near or along the ventricle borders, and
383 exhibited characteristics reminescent of an immature phenotype, e.g. a circular shape with few and short
384 cellular processes (**Figure 8-supplement 1**). In this mutant, the density of GFP^{-}; Lcp1^{+} DC-like cells was
385 reduced in comparison to *wild-type* controls, in the ventral area (~50%) (**Figure 8U,W**).

386 As well-established regulators of zebrafish microglia, *csf1ra* or *csf1rb* deficiency had a strong effect on
387 GFP^{+}; Lcp1^{+} cells, with densities decreased ~50% in the dorsal and ventral areas. Interestingly, the density
388 of GFP^{-}; Lcp1^{+} DC-like cells was reduced in the ventral part of *csf1rb* homozygous fish (~50%), while it was
389 doubled in *csf1ra*$^{-/-}$ mutant animals in comparison to *wild-type* siblings (**Figure 8I-P, U,W**). Finally, we also
390 examined fish lacking both *csf1r* paralogs (*csf1r*^{DM}). These fish displayed a more severe phenotype, being
391 mostly devoid of both populations of microglia and DC-like cells, as indicated by the absence of GFP and
392 Lcp1 signal (**Figure 8Q-W**). This is consistent with previous reports that *mpeg1:GFP*$^{+}$ cells are depleted in
393 the brain of *csf1r*^{DM} fish (Ferrero et al. 2021; Oosterhof et al. 2018).

394 Collectively, these results demonstrate the different mononuclear phagocyte-deficient zebrafish mutant
395 lines have reduced numbers of microglia and exhibit distinct DC-like cell phenotypes. Our data also reveal
396 that DC-like cells develop in an *irf8*-dependant manner, and identify possible opposite functions for the
397 *csf1r* paralogs in the maintenance of this population.

398

399 **DISCUSSION**

400 In the present study, we have characterized the immune microenvironment of the adult zebrafish brain
401 by profiling total cd45^{+} leukocytes, isolated from transgenic reporter fish by FACS. First we show that, like
402 in mammals, microglia constitute the predominant parenchymal immune cell in the brain of the adult
403 zebrafish. Zebrafish microglia are identified based on several common canonical markers, some of which
404 are previously reported to be conserved in mammals (Mazzolini et al. 2019; Silva et al. 2021; Oosterhof et
405 al. 2018). These include *apoeb*, *apoc1*, *lgals3bpb*, *ccl34b.1* and *p2ry12*. Notably, we used different
406 combinations of fluorescent reporter lines for the prospective isolation of adult microglia and found these
407 genes to be consistently expressed. In addition, our observations also support a phenotypical

408 heterogeneity of adult zebrafish microglia in the steady state by identifying several clusters sharing this
409 microglia core signature, with different expression levels. This is in line with recent advances in our
410 understanding of microglia diversity in human and mouse, and which revealed the presence of
411 molecularly distinct microglia subtypes across developmental stages, specific brain regions or disease
412 conditions (Stratoulias et al. 2019; Masuda et al. 2020).

413 Although the notion of microglia heterogeneity in zebrafish is already proposed (Silva et al. 2021; Wu et
414 al. 2020), a major finding of our study is that, surprisingly, not all parenchymal mononuclear phagocytes
415 qualify as microglial cells. Here we provide evidence that a proportion of myeloid cells in the healthy brain
416 parenchyma is phenotypically distinct from microglia and identify as the zebrafish counterpart of
417 mammalian cDC1. These cells, despite sharing the microglial expression of *mpeg1.1* and genes involved
418 in antigen presentation, display a unique transcriptomic profile characterized by a core gene signature
419 resembling that of mammalian cDC1 (*flt3*$^{+}$*, irf8*^{high}*, batf3*$^{+}$*, id2*$^{+}$*, xcr1*$^{+}$) but lacking canonical microglia
420 markers. The lineage identity of these cells (referred to as DC-like cells), is further supported by their
421 dependency to *batf3*, a key transcription factor for cDC1 development in mammals. In contrast, zebrafish
422 microglia develop normally in absence of *batf3*, which highlights the reliance of both populations on
423 distinct developmental programs. This notion is also reinforced by demonstrating that, unlike microglia,
424 zebrafish brain DC-like cells are *csf1ra*-independant. However, both populations are controlled by *irf8*, a
425 well-established regulator of microglia differentiation and DC development in mammals (Van Hove et al.
426 2019; Cabeza-Cabrerizo et al. 2021).
427

428 Previously, two independent studies have reported the existence of an immune cell population with a
429 similar expression profile to DC-like cells in the juvenile and adult zebrafish brain (Wu et al. 2020; Silva et
430 al. 2021). However, contradictory conclusions were drawn regarding the identity of these cells. In one
431 study using bulk RNAseq, a cell population expressing *id2a*, *ccl19a.1*, *siglec15l*, but not *apoeb* or *lgals3bpb*,
432 was identified and categorized as a phenotypically distinct microglia subtype (Wu et al. 2020). This
433 population could be discriminated from other *mpeg1*-expressing parenchymal cells notably by the lack of
434 Tg(*ccl34b.1:GFP*) transgene expression. Interestingly, while *ccl34b.1*$^{+}$; *mpeg1*$^{+}$ microglia were widely
435 spread across brain regions, *ccl34b.1*$^{-}$ *mpeg1*$^{+}$ cells showed a restricted spatial localization in the white
436 matter. In addition, these cells also displayed a highly ramified morphology as well as independency of
437 *csf1ra* signaling, all reminescing the DC-like cells identified in our study. However, in another report using
438 single-cell RNAseq, a comparable myeloid population expressing high levels of *mpeg1* as well as *ccl19a.1*,
439 *flt3*, *siglec15l*, among other DC-like genes, was labeled as brain macrophages, owing to the absence of
440 microglial-specific markers such as *p2ry12*, *csf1ra*, *hexb* and *slc7a7* (Silva et al. 2021). The present work
441 resolves these apparent contradictions, and provides new insights into the identity of this cell population.
442 We report here that *ccl34b.1*$^{-}$*; mpeg1*$^{+}$ cells display a similar gene signature to the DC-like cells identified
443 in our analyses. This strongly suggests that the *ccl34b.1*$^{-}$*; mpeg1*$^{+}$ and *p2ry12*$^{-}$*; mpeg1*$^{+}$ populations share
444 a similar cellular identity. Likewise, the anatomical location of the brain macrophage cluster identified by
445 Silva and colleagues was not investigated, but based on their dominated expression profile by key DC
446 markers, these cells likely represent the equivalent of the *p2ry12*$^{-}$*; mpeg1*$^{+}$ cell population. Thus, based
447 on the evidence that these three populations constitute a unique cell type, and coupled to the
448 demonstration that *in vivo p2ry12*$^{-}$*; mpeg1*$^{+}$ cells are reliant on *batf3*, collectively these features imply
449 these cells share more similarities with mammalian DCs than with microglia or macrophages. Therefore,
450 based on their distinct morphology, transcriptomic signature, and *batf3*-dependency, we propose that
451 this population represents DC-like cells rather than microglia or macrophages. Importantly, since the

452 submission of our manuscript, the Wen lab published an independent study in which they now reclassify
453 the ccl34b.1^{-} mpeg1^{+} cells in the zebrafish brain as cDCs, thus revising their earlier interpretation of these
454 cells as microglia (Zhou et al. 2023).

455 One important question raised from these new findings could relate to the abundance of DC-like cells
456 within the healthy zebrafish brain parenchyma, which is strongly different than what is known in
457 mammals. Indeed, while murine DCs are naturally found at the brain border regions such as the meningeal
458 layers and the choroid plexus (structures in contact with the brain microenvironment) (Van Hove et al.
459 2019) their presence within the healthy brain parenchyma is scarce and somewhat controversial. In
460 mammals, infiltration of functional DCs in the brain parenchyma occurs with age (Kaunzner et al. 2012),
461 or following an injury or infection, where they act as important inducers of the immune response through
462 activation of primary T cells and cytokine production (Ludewig et al. 2016). In addition, DC infiltration is a
463 hallmark of several neurological diseases and aging, and is believed to contribute to the establishment of
464 a chronic neuroinflammatory state (Ludewig et al. 2016). In this regard, Wu et al. previously reported that
465 *ccl34b.1^{-} mpeg1^{+}* cells - or DC-like cells - exhibit functional differences, including limited mobility and
466 phagocytic properties, and enhanced release of immune regulators following bacterial infection, when
467 compared to *ccl34b.1^{+} mpeg1^{+}* microglia. The same study also proposed that zebrafish *ccl34b.1^{-}; mpeg1^{+}*
468 cells might play a regulatory role by recruiting T lymphocytes in the brain parenchyma upon infection (Wu
469 et al. 2020). These biological features suggest that brain DC-like cells might exibit APC functions. However,
470 due to a lack of tools this hypothesis is currently difficult to address. There is evidence that DC
471 functionalities are conserved in teleosts (Lugo-Villarino et al. 2010; Bassity and Clark 2012), but the
472 process of antigen presentation in zebrafish remains poorly understood (Lewis, Del Cid, and Traver 2014).
473 Because zebrafish lack apparent lymph nodes and the secondary lymphoid structures found in mammals,
474 it is not known where stimulation of naive T cells takes place and whether fish have developped unique
475 ways to mount an adaptive immune response. Therefore, although a comprehensive analysis of the
476 anatomical zone enriched in DC-like cells requires further investigation, from an evolutionary perspective,
477 it is tempting to speculate that the specific localization of zebrafish DC-like cells in the ventral brain tissue
478 might provide an environment to facilitate antigen detection and/or presentation in this organ. Future
479 work using the mutants as described in this study in addition to new DC-like-specific reporter lines will
480 help addressing such exciting questions.

481 Furthermore, our work sheds light on the myeloid brain phenotype of mutant lines commonly used by
482 the fish macrophage/microglia community. CSF1R is a master regulator of macrophage development and
483 function in vertebrates which is found in two copies (*csf1ra* and *csf1rb*) in zebrafish due to an extra
484 genome duplication. Others and we have contributed to the uncovering of the relative contribution of
485 each paralog to the ontogeny of zebrafish mononuclear phagocytes (Herbomel, Thisse, and Thisse 2001;
486 Ferrero et al. 2021; Hason et al. 2022; Oosterhof et al. 2018). Here we also provide a new level of precision
487 regarding these processes. As reported, the density of all parenchymal *mpeg1:GFP^{+}* mononuclear
488 phagocytes is reduced in the brain of single *csf1ra$^{-/-}$* and *csf1rb$^{-/-}$* adult mutant fish, and these cells
489 disappear when both genes are knocked out (Oosterhof et al. 2018; Ferrero et al. 2021). Using *in vivo*
490 lineage tracing, we previously demonstrated that zebrafish microglia are established in two successive
491 steps, with a definitive wave of hematopoietic stem cell (HSC)-derived adult microglia replacing an
492 embryonic/primitive population. In addition, we showed that in *csf1rb$^{-/-}$* fish remaining *mpeg1:GFP^{+}* cells
493 are of primitive origin, whereas in *csf1ra$^{-/-}$* fish they are of definitive origin (Ferrero et al. 2021).
494 Collectively, these observations have led to a model in which embryonic-derived microglia make up the

majority of remaining *mpeg1*-expressing cells in *csf1rb*$^{-/-}$ fish, while residual cells represent adult microglia in the *csf1ra*$^{-/-}$ line, but at a strongly reduced cell number relative to controls. However, adult microglia in these experiments were identified based on the concomitant *mpeg1:GFP* transgene expression and the HSC lineage tracing marker, a strategy that, retrospectively, did not allow to discriminate them from the DC-like cells described in this study. Here, we sought to test these models in light of our current findings, and especially following the observation that individual mutant fish exhibit opposite brain DC-like phenotypes, with DC-like cell numbers being strongly increased or decreased in *csf1ra*$^{-/-}$ and *csf1rb*$^{-/-}$ animals, respectively. In mammals, DCs arise from HSCs in the bone marrow. Although the developmental origin of zebrafish brain DC-like cells remains uncharacterized, their reduced numbers in the *csf1rb* mutant, despite their lack of *csf1rb* expression, likely reflects impaired HSC-derived definitive myelopoiesis, in line with the current model in which *csf1rb* acts at the progenitor level in the WKM to promote myeloid lineage commitment (Ferrero et al. 2021; Hason et al. 2022). Accordingly, the *csf1rb*$^{-/-}$ line is devoid of both populations of adult microglia and DC-like cells and, as initially proposed, the most residual cells within the brain parenchyma represent remnants of embryonic microglia (Ferrero et al. 2021). Conversely, the increased density of DC-like cells in *csf1ra*$^{-/-}$ adult fish indicates that this paralogue is dispensable for the ontogeny of DC-like cells, but points to a possible role (likely indirect) in controlling the DC-like cell growth and/or survival. This is in contrast with microglia, which we now found to be unambiguously depleted following a *csf1ra* loss-of-function. Therefore, these findings warrant an adjustment of the initial model, as the majority of remaining *mpeg1*-expressing cells in the *csf1ra*$^{-/-}$ line correspond to DC-like cells, and not adult microglia. Notably, these results are consistent with the reported loss of *ccl34b.1*$^{+}$; *mpeg1*$^{+}$ cells in *csf1ra*$^{-/-}$ fish by Wu and colleagues (Wu et al. 2020), and with the observed upregulation of DC-like genes coupled to a downregulation of microglia markers in *mpeg1*:GFP cells isolated from the brain of *csf1ra*$^{-/-}$ *csf1rb*$^{+/-}$ mutant animals (Oosterhof et al. 2018).

In zebrafish little is known regarding lymphoid cells in the adult CNS. Similar to DCs, lymphocytes are present in limited numbers in the healthy mammalian brain and mainly restricted to the meningeal layers, choroid plexus or the perivascular space (Mundt et al. 2019; Croese, Castellani, and Schwartz 2021). In our transcriptomic analysis, we identified an heterogenous repertoire of lymphoid cells: T, NK and ILCs. B lymphocytes, which could not be captured using the *cd45:DsRed* transgene (Wittamer et al. 2011), were also detected using the *IgM*:GFP line, albeit in very low numbers. Our data suggest that, similar to mammals, in zebrafish lymphoid cells in the steady-state are only occasionally found in the brain parenchyma, and are most likely localized in the brain border regions. Here, it is worth noting that our protocol for brain dissection requires the removal of the skull, which may completely or partially disrupt the thin meningeal layers. Consequently, whether non parenchymal cells identified in this study are located in the meninges, in the choroid plexus or even in the blood circulation remains to be determined.

Although the innate counterparts of the lymphoid system (NK cells and ILCs) have been identified in different zebrafish organs (Hernández 2018; Silva et al. 2021; Tang et al. 2017), the lack of specific fluorescent reporter lines has until now precluded a detailed characterization of these cell populations. In particular, as a recently discovered cell type in zebrafish (Hernández 2018), the phenotypic and functional heterogeneity of ILC-like cells are still poorly understood. In this study, we found that the adult zebrafish brain contains a population that resembles the ILC2 subset in mammals. Like human and mouse ILC2s, these cells do not express *cd4-1*, the co-receptor for the T cell receptor (TCR). However, they are positive for T_H2 cytokines *il13* and *il4*, and also express *gata3*, a transcription factor involved in ILC2 differentiation. Surprisingly, *lck* expression in our dataset was restricted to T lymphocytes and NK cells, whereas in

538 humans, this gene is expressed across all ILC subsets (Bjorklund et al. 2016). A previous study in zebrafish
539 reported populations representing all three ILC subtypes isolated from the intestine based on expression
540 of the *lck:GFP* transgene (Hernández 2018). That suggests a conserved *lck* expression pattern across
541 species. However, in none of these experiments the presence of ILCs in the *lck:GFP* negative fraction was
542 investigated, so whether the absence of *lck* transcripts in our ILC2 dataset is due to a low detection
543 sensitivity or a lack of expression remains an open question. Nevertheless, as we showed, the level of
544 expression of ILC2 transcripts remain specifically unchanged in brain leukocytes in the context of T cell
545 deficiency. This validates that ILC2 are indeed present in this organ. In line with this, innate-lymphoid-like
546 cells differentially expressing *il4*, *il13* and *gata3* have been recently annotated in the juvenile zebrafish
547 brain (Silva et al. 2021).

548 To conclude, our study provides a single-cell transcriptomic dataset of different brain leukocyte
549 populations, and may serve as a reference to better characterize the immune cell complexity of the
550 zebrafish brain in the steady state. Similar to mammalian microglia, zebrafish microglia are identified
551 based on several common canonical markers, some of which are conserved between species, but their
552 diversity is still poorly understood. Therefore, future investigations will benefit from mapping microglia
553 heterogeneity across the zebrafish brain as a complementary approach to single-cell transcriptomics for
554 studying microglia functions in health and disease. Further work will also be needed to elucidate the
555 functions of some of the cell types identified in this study, especially DC-like cells, and to elucidate whether
556 this population maintains locally or is continually replenished by cells from the periphery.

557

558 **MATERIALS AND METHODS**

559 **Zebrafish husbandry**

560 Zebrafish were maintained under standard conditions, according to FELASA (Alestrom et al. 2019) and
561 institutional (Université Libre de Bruxelles, Brussels, Belgium; ULB) guidelines and regulations. All
562 experimental procedures were approved by the ULB ethical committee for animal welfare (CEBEA) from
563 the ULB. The following lines were used: *Tg(mhc2dab:GFP$_{LT}$)^{sd67}* (Wittamer et al. 2011),
564 *Tg(ptprc:DsRed^{express})^{sd3}* (here referred to as *cd45:DsRed*) (Wittamer et al. 2011), *Tg(mpeg1.1:eGFP)^{gl22}*
565 (here referred to as *mpeg1:GFP*) (Ellett et al. 2010), *Tg(mpeg1.1:mCherry)^{gl23}* (here referred to as
566 *mpeg1:mCherry*) (Ellett et al. 2010), *TgBAC(p2ry12:p2ry12-GFP)^{hdb3}* (Sieger et al. 2012), *Tg(lck:lck-eGFP)^{cz1}*
567 (here referred to as *lck:GFP*) (Langenau et al. 2004), *TgBAC(cd4-1:mcherry)^{UMC13}* (here referred to as *cd4-*
568 *1:mCherry*) (Dee et al. 2016), *Tg(Cau.Ighv-ighm:EGFP)^{sd19}* (here referred to as *ighm:GFP*) (Page et al. 2013),
569 *Tg(mpx:GFP)^{i113}* (Mathias, Walters, and Huttenlocher 2009). The mutant lines used were: *panther^{i4e1}* (here
570 called *csf1ra$^{-/-}$*)(Parichy DM 2000); *csf1rb^{sa1503}*, generated via ethyl-nitrosurea (ENU) mutagenesis, were
571 obtained from the Sanger Institute Zebrafish Mutation Project and previously characterized (Ferrero et al.
572 2021), *irf8^{std96}* (Shiau et al. 2015), *rag2^{E450fs}* (Tang et al. 2014). Special care was taken to control reporter
573 gene dosage through experiments (with all control and mutant animals used in this study known to carry
574 similar hemizygous or homozygous doses of the GFP transgenes). The term "adult" fish refers to animals
575 aged between 4 months and 8 months old. For clarity, throughout the text, transgenic animals are
576 referred to without allele designations.

577

578 **Generation of *batf3*$^{-/-}$ mutant zebrafish**

579 The *batf3* (ENSDARG00000042577) knockout mutant line was generated using the CRISPR/Cas9 system.
580 A single guide RNA (sgRNA) targeting the ATG start in the first exon (targeting sequence:
581 GAAGTGATGCTCCAGCTCTA) was identified and selected for its highest on-target activity and lowest
582 predicted off-target score using a combination of the Sequence Scan for CRISPR software (available at
583 http://crispr.dfci.har- vard.edu/SSC/) (Xu et al. 2015) and the CRISPR Scan (available at
584 http://www.crisprscan.org/). The DNA template for the sgRNA synthesis was produced using the PCR-
585 based short-oligo method as described (Talbot and Amacher 2014). The following primers were used: Fw:
586 5'- GCGATTTAGGTGACACTATA-3' and Rv: 5'- AAAGCACCGACTCGGTGCCAC-3'. The resulting PCR product
587 was purified by phenol-chloroform extraction and used for *in vitro* transcription using SP6 RNA-
588 polymerase (NEB, M0207). The resulting sgRNA was purified using the High Pure PCR Cleanup Microkit
589 (Roche, 498395500). 60 pg sgRNA and 100 pg Cas9 protein (PNA Bio) were co-injected into one-cell stage
590 *wild-type* embryos. The genotyping of both embryos and adults was performed using the following
591 primers: *batf3* fw: 5'- ACTTGACAGTTTAAGCATGCCT-3' and *batf3* rv: 5'- GAACATACCTCGCTCTGTCG-3'.
592 PCR amplicons were analyzed using a heteroduplex mobility assay (on a 8% polyacrylamide gel) to assess
593 the presence of CRISPR/Cas9-induced mutations.

594 The *batf3*^{ulb31} line carries an 8-bp deletion in exon 1. The deletion introduces a frameshift after amino acid
595 16 of the predicted 121-amino acid ORF, followed by 8 heterologous amino acids and then three
596 successive premature stop codons. Heterozygous F1 fish were backcrossed at least four generations with
597 AB* *wild-types* before being crossed to *Tg(mhc2dab:GFP; cd45:DsRed)* fish, as well as *Tg(p2ry12:p2ry12-*
598 *GFP; mpeg1:mCherry)* animals for phenotype assessment.

599

600 **Flow cytometry and cell sorting**

601 Cell suspensions from adult brains were obtained as previously described (Wittamer et al. 2011; Ferrero
602 et al. 2021; Ferrero et al. 2018). Briefly, adult brains dissected in 0.9X Dulbecco's Phosphate Buffered
603 Saline (DPBS) were triturated and treated with Liberase TM at 33°C for 30-45 minutes, fully dissociated
604 using a syringe with a 26G needle and washed in 2% fetal bovine serum diluted in 0.9X DPBS. Cell
605 suspensions were centrifuged at 290g 4ºC 10 min and filtered through a 40µm nylon mesh. Just before
606 flow cytometry analysis, SYTOX™Red (Invitrogen) was added to the samples at a final concentration of
607 5nM to exclude non viable cells. Flow cytometry acquisition and cell sorting was performed on a FACS
608 ARIA II (Becton Dickinson). To perform the qPCR experiments, between 7,000-10,000 *cd45:DsRed+*
609 leukocytes and approximately 2,500 *p2ry12:GFP*$^{+}$*; mpeg1:mCherry*$^{+}$ microglia or *p2ry12:GFP*$^{-}$*;*
610 *mpeg1:mCherry*$^{+}$ DC-like cells were sorted, collected in RLT Plus buffer (Qiagen) and flash freezed in liquid
611 nitrogen. Analyses were performed using FlowJo software. For morphological evaluation, 100,000
612 *cd45*:DsRed^{+} sorted cells were concentrated by cytocentrifugation at 300g for 10 minutes onto glass slides
613 using a Cellspin (Tharmac). Slides were air-dried, fixed with methanol for 5 minutes and stained with May-
614 Grünwald solution (Sigma) for 10 minutes. Then, slides were stained with a 1:5 dilution of Giemsa solution
615 (Sigma) in distilled water (dH_2O) for 20 minutes, rinsed in dH_2O, dehydrated through ethanol series and
616 mounted with DPX (Sigma).

617

618 **Bulk RNA sequencing and data analysis**

619 **Sample processing and cDNA.** Cell sorting and RNA sequencing was performed as previously described
620 (Kuil et al. 2020). Approximately 8,000 microglial cells (*p2ry12*$^{+}$*; cd45*$^{+}$ or *mhc2dab*$^{+}$*; cd45*^{low}, n=2 for each
621 Tg) and 1,200 DC-like cells (*mhc2dab*$^{+}$*; cd45*^{high}, n=2) were sorted. RNA was isolated using the miRNeasy
622 Micro Kit (Qiagen) according to the manufacturer's instructions. RNA concentration and quality were
623 evaluated using a Bioanalyzer 2100 (Agilent technologies). The Ovation Solo RNA-Seq System (NuGen-
624 TECAN) with the SoLo Custom AnyDeplete Probe Mix (Zebrafish probe set) were used to obtain indexed
625 cDNA libraries following manufacturer recommendation. **Sequencing.** Sequencing libraries were loaded
626 on a NovaSeq 6000 (Illumina) using a S2 flow cell and reads/fragments were sequenced using a 200 Cycle
627 Kit. **Alignment and feature counting.** Sequenced reads were then trimmed using *cutadapt* with default
628 parameters except for "--overlap 5 --cut 5 --minimum-length 25:25 -e 0.05". Trimmed FQ files were at this
629 point processed with the same approach for both datasets, including Wu et al. 2021 expression data that
630 were retrieved from GEO data repository (GEO Accession: GSM4725741) (Wu et al. 2020). Trimmed and
631 filtered reads were then mapped against the reference genome GRCz11.95 using STAR aligner with the "–
632 twopassMode basic" and "–sjdbOverhang 100". BAM files were then indexed and filtered using
633 SAMTOOLS "view -b -f 3 -F 256". Finally, transcript feature annotations for Ensembl genes using
634 *Danio_rerio* v. GRCz11.95 were quantified using HTSeq-counts call with default parameters specifying "-r
635 pos -s yes -a 10 --additional-attr=gene_name -m intersection-nonempty --secondary-alignments=ignore -
636 -supplementary-alignments=ignore". General sequencing and mapping stats were calculated using fastqc
637 and multiQC. **Feature count matrix preprocessing, normalization and differential expression.** Feature
638 count matrices were further preprocessed filtering low count genes (>=10#) for 2 out of 2 samples in each
639 group (this manuscript dataset) or 3 out of 5 samples per group (Wu et al. 2020 dataset). Overall, for this
640 manuscript dataset, we obtained 13663 genes expressed in both replicates whereas Wu et al. 2020
641 dataset, showed 9007 genes that were expressed in at least 3 of the 5 replicates. Then DESeq2 (v. 1.30.0)
642 for R statistical computing was used to normalize the raw counts and perform differential expression
643 analysis focussing on protein-coding genes with de-duplicated gene names (as "_#") (Love, Huber, and
644 Anders 2014). Statistical differential expression and downstream analyses were performed using R
645 Statistical software v. 4.0.3.

646

647 **Single-cell RNA sequencing and data analysis**

648 **Single-Cell RNA-seq library preparation and sequencing.** Adult brain single-cell suspensions were
649 prepared as described before from adult *Tg(p2ry12:GFP; cd45:DsRed)* fish (n=3), using calcein violet to
650 exclude dead cells (1µM, Thermo Fisher). A total of 14,000 *cd45:DsRed*$^{+}$ cells were processed for single-
651 cell profiling using the 10x Genomics platform and diluted to a density of 800 cells/µl following 10x
652 Genomics Chromium Single cell 3' kit (v3) instructions. Library preparation was performed according to
653 10x Genomics guidelines and sequenced on an Illumina NextSeq 550. Raw sequencing data was processed
654 using the Cell Ranger with a custom-built reference based on the zebrafish reference genome GRCz11 and
655 gene annotation Ensembl 92 in which the EGFP and DsRed sequence were included.

656 **Single-cell RNA-seq data preprocessing.** Single cell raw counts were processed using Seurat (v3)(Butler et
657 al. 2018; Satija et al. 2015). Briefly, genes with zero counts for all cells were removed, and applied cell
658 filters for >=20% reads mapping to mitochondrial genes and nFeature >300. Additionally, mitochondrial
659 genes '^mt-' and ribosomal genes '^rp[sl]' were masked for further downstream analysis, as well as non-
660 coding protein genes selected with the current feature annotations of the EnsemblGene 95 from GRCz11

661 zebrafish genome. Overall, providing a dataset of 4,145 cells and 18,807 genes for single cell data analysis.
662 Analysis using the *scDblFinder R*
663 *package (https://rdrr.io/bioc/scDblFinder/f/vignettes/2_scDblFinder.Rmd*) found no evidence of doublet
664 enrichment, indicating that the clusters were sufficiently robust to capture normal cell states. **Single-Cell**
665 **Normalization, clustering and marker genes.** Single-cell filtered data were normalized using Seurat's
666 SCTransform method with the following custom parameters: "variable.features.n=4000 and
667 return.only.var.genes=F". Then, the nearest neighbour graph was built with 40 PCA dimensions, and
668 clusters were identified using manually selected resolution based on the supervised inspection of know
669 markers leading to the optimal "resolution= 0.6 (Louvain)" and "n.neighbors=20". The same parameters
670 were used for the dimensionality reduction as UMAP. Finally, cluster annotation was performed by
671 inspecting the identified marker genes using FindAllMarkers function (one v. rest with default parameters
672 except for "min.pct=0.25"". **Single Cell Pathway analysis.** For pathway analysis, marker genes of all four
673 microglia clusters together (MG1, MG2, MG3, MG4) or all four DC-like clusters (DC1, DC2, DC3, DC4) were
674 obtained using Seurat's FindMarkers function. Next, differentially expressed zebrafish genes (log2 fold-
675 change >0.25, P-adjusted < 0.05) were converted to their human orthologs using gProfiler tool (Raudvere
676 et al. 2019) and validated using the ZFIN (zfin.org) and Alliance Genome databases
677 (www.alliancegenome.org). Genes with no corresponding orthologs were not included. From this gene
678 lists, Gene ontology terms (Biological Processes) and Reactome pathways were obtained using the
679 Cytoscape ClueGO application (two-sided hypergeometric statistical test, Bonferroni correction)(Bindea
680 et al. 2009). To explore MG and DC-like conserved cell type signatures (**Table 4**), each gene list was
681 uploaded to the Enrichr databas (Xie et al. 2021) to identify the most enriched "Cell Types" categories
682 querying PanglaoDB (Franzen, Gan, and Bjorkegren 2019).

683

684 **Quantitative PCR**

685 RNA extraction was performed using the RNeasy Plus Mini kit (Qiagen) and cDNAs were synthesized using
686 the qscript cDNA supermix (Quanta Biosciences), as previously described (Ferrero et al. 2018). Reactions
687 were run on a Bio-Rad CFX96^{TM} real time system (Bio-Rad), using the Kapa SYBR Fast qPCR Master Mix
688 (2X) kit (Kapa Biosystems) under the following thermal cycling conditions: 3 min at 95°C and 40 cycles of
689 5 s at 95°C, 30 s at 60°C. A final dissociation at 95ºC for 10 s and a melting curve from 65 to 95°C (0.5°C
690 increase every 5 s) were included to verify the specificity and absence of primer dimers. Biological
691 replicates were compared for each subset. Relative amount of each transcript was quantified via the ΔCt
692 method, using *elongation-Factor-1-alpha* (*eef1a1l1*; ENSDARG00000020850) expression for
693 normalization.

694

695 **Immunostaining and vibratome sections**

696 Adult brains were dissected, fixed in 4% PFA, and incubated overnight in 30% sucrose in PBS before being
697 snap-frozen in OCT (Tissue-Tek, Leica) and stored at -80°C. Immunostaining was performed on 14 µm
698 cryosections as previously described (Ferrero et al. 2018). The following primary and secondary antibodies
699 were used: chicken anti-GFP polyclonal antibody (1:500; Abcam, Cat# ab13970), rabbit anti-Lcp1 (1:1000),
700 mouse anti-mCherry monoclonal antibody (1:500; Takara Bio Cat# 632543), Alexa Fluor 488-conjugated
701 anti-chicken IgG antibody (1:500; Abcam Cat# ab150169), Alexa Fluor 594- conjugated anti-rabbit IgG

(1:500; Abcam Cat# ab150076), Alexa Fluor 647-conjugated anti-mouse IgG (1:500; Abcam Cat# ab150107). For vibratome sections, adult brains were fixed in 4% PFA, embedded in 7% low-melting agarose in PBS, and sectioned at 100 µm using a vibratome (Leica). Sections were mounted directly with Glycergel (Dako) and imaged without prior immunostaining to visualize endogenous *cd45:DsRed* fluorescence.

Imaging and image analyses

Fluorescent samples were imaged using a Zeiss LSM 780 inverted microscope (Zeiss, Oberkochen, Germany), with a Plan Apochromat 20X objective. Image post-processing was performed using Zeiss Zen Software (ZEN Digital Imaging for Light Microscopy), as previously described (Ferrero et al. 2021). Cells were manually counted using the Black Zen software and divided by the area of the brain section (cell density/μm^2) and quantified between 5-11 transversal sections per brain. Cytospuned cells were imaged using a Leica DM 2000 microscope equipped with a 100X objective, and scanned using a NanoZoomer-SQ Digital Slide scanner (Hamamatsu).

Data collection

The sample size was chosen based on previous experience in the laboratory, for each experiment to yield high power to detect specific effects. No statistical methods were used to predetermine sample size and experiments were repeated at least twice. Homozygous mutant animals used in this study were obtained by heterozygous mating. No fish were excluded. Genotyping was performed on tail biopsies collected from individual euthanized fish, in parallel to brain dissection. Randomly selected samples for each genotype were then immunostained in one batch, assessed phenotypically in a blind manner and grouped based on their genotype.

Statistical analyses

Statistical differences between mean values of two experimental groups were analyzed by Student's t-test or the equivalent U-Mann-Whitney non-parametric test, when parametric assumptions were not met in the sample data. Results are expressed as mean ± standard of the mean (SEM) and considered to be significant at $P < 0.05$. Details on the number of fish (biological replicates) used in each experiment, the statistical test used and statistical significance are indicated in each figure and figure legends. Statistical analyses were performed using GraphPad Prism8.

ACKNOWLEDGEMENTS

We thank all members of the Wittamer lab and Sumeet Pal Singh for critical discussion and comments on the manuscript. We are also grateful to Marianne Caron for technical assistance and to Daniel M. Borràs for guidance with bioinformatic analyses. We also aknowledge Christine Dubois for support with flow cytometry, F. Libert and A. Lefort from the ULB Genomic Core Facility and S. Reinhardt, A. Kränkel and A. Petzold at the Dresden-Concept Genome center in Germany.

COMPETING INTERESTS

The authors declare no competing financial interests.

FUNDING

This work was funded in part by the Funds for Scientific Research (FNRS) under Grant Numbers F451218F, UN06119F and UG03019F, the program ARC from the Wallonia-Brussels Federation, the Minerve Foundation (to V.W.), the Fonds David et Alice Van Buuren, the Fondation Jaumotte-Demoulin and the Fondation Héger-Masson (to V.W. , G.F. and M.M.). M.R. is supported by a Chargé de Recherche fellowship (FNRS), G.F. and A.M. by a Research Fellowship (FNRS) and M.M. by a fellowship from The Belgian Kid's Fund.

DATA AVAILABILTY STATEMENT

All datasets and material generated for this study are included in the manuscript/ Supplementary Files and will be shared upon request. Raw data for single cell RNA-seq samples and RNA-seq are available in the ArrayExpress database as accession number E-MTAB-13223 and E-MTAB-13228, respectively. The transcriptomic atlas generated in this study is available as a searchable database at: *https://scrna-analysis-zebrafish.shinyapps.io/scatlas/*

REFERENCES

Alestrom, P., L. D'Angelo, P. J. Midtlyng, D. F. Schorderet, S. Schulte-Merker, F. Sohm, and S. Warner. 2019. 'Zebrafish: Housing and husbandry recommendations', *Lab Anim*: 23677219869037.

Alves de Lima, K., J. Rustenhoven, S. Da Mesquita, M. Wall, A. F. Salvador, I. Smirnov, G. Martelossi Cebinelli, T. Mamuladze, W. Baker, Z. Papadopoulos, M. B. Lopes, W. S. Cao, X. S. Xie, J. Herz, and J. Kipnis. 2020. 'Meningeal gammadelta T cells regulate anxiety-like behavior via IL-17a signaling in neurons', *Nat Immunol*, 21: 1421-29.

Bassity, E., and T. G. Clark. 2012. 'Functional identification of dendritic cells in the teleost model, rainbow trout (Oncorhynchus mykiss)', *PLoS One*, 7: e33196.

Bindea, G., B. Mlecnik, H. Hackl, P. Charoentong, M. Tosolini, A. Kirilovsky, W. H. Fridman, F. Pages, Z. Trajanoski, and J. Galon. 2009. 'ClueGO: a Cytoscape plug-in to decipher functionally grouped gene ontology and pathway annotation networks', *Bioinformatics*, 25: 1091-3.

Bjorklund, A. K., M. Forkel, S. Picelli, V. Konya, J. Theorell, D. Friberg, R. Sandberg, and J. Mjosberg. 2016. 'The heterogeneity of human CD127(+) innate lymphoid cells revealed by single-cell RNA sequencing', *Nat Immunol*, 17: 451-60.

Bottcher, C., S. Schlickeiser, M. A. M. Sneeboer, D. Kunkel, A. Knop, E. Paza, P. Fidzinski, L. Kraus, G. J. L. Snijders, R. S. Kahn, A. R. Schulz, H. E. Mei, N. B. B. Psy, E. M. Hol, B. Siegmund, R. Glauben, E. J. Spruth, L. D. de Witte, and J. Priller. 2019. 'Human microglia regional heterogeneity and phenotypes determined by multiplexed single-cell mass cytometry', *Nat Neurosci*, 22: 78-90.

Butler, A., P. Hoffman, P. Smibert, E. Papalexi, and R. Satija. 2018. 'Integrating single-cell transcriptomic data across different conditions, technologies, and species', *Nat Biotechnol*, 36: 411-20.

Butovsky, O., M. P. Jedrychowski, C. S. Moore, R. Cialic, A. J. Lanser, G. Gabriely, T. Koeglsperger, B. Dake, P. M. Wu, C. E. Doykan, Z. Fanek, L. Liu, Z. Chen, J. D. Rothstein, R. M. Ransohoff, S. P. Gygi, J. P. Antel, and H. L. Weiner. 2014. 'Identification of a unique TGF-beta-dependent molecular and functional signature in microglia', *Nat Neurosci*, 17: 131-43.

Butovsky, O., and H. L. Weiner. 2018. 'Microglial signatures and their role in health and disease', *Nat Rev Neurosci*, 19: 622-35.

Cabeza-Cabrerizo, M., A. Cardoso, C. M. Minutti, M. Pereira da Costa, and E. Sousa C. Reis. 2021. 'Dendritic Cells Revisited', *Annu Rev Immunol*, 39: 131-66.

Carmona, S. J., S. A. Teichmann, L. Ferreira, I. C. Macaulay, M. J. Stubbington, A. Cvejic, and D. Gfeller. 2017. 'Single-cell transcriptome analysis of fish immune cells provides insight into the evolution of vertebrate immune cell types', *Genome Res*, 27: 451-61.

Carradice, D., and G. J. Lieschke. 2008. 'Zebrafish in hematology: sushi or science?', *Blood*.

Croese, T., G. Castellani, and M. Schwartz. 2021. 'Immune cell compartmentalization for brain surveillance and protection', *Nat Immunol*, 22: 1083-92.

D'Amora, M., A. Galgani, M. Marchese, F. Tantussi, U. Faraguna, F. De Angelis, and F. S. Giorgi. 2023. 'Zebrafish as an Innovative Tool for Epilepsy Modeling: State of the Art and Potential Future Directions', *Int J Mol Sci*, 24.

Dee, C. T., R. T. Nagaraju, E. I. Athanasiadis, C. Gray, L. Fernandez Del Ama, S. A. Johnston, C. J. Secombes, A. Cvejic, and A. F. Hurlstone. 2016. 'CD4-Transgenic Zebrafish Reveal Tissue-Resident Th2- and Regulatory T Cell-like Populations and Diverse Mononuclear Phagocytes', *J Immunol*, 197: 3520-30.

Drieu, A., S. Du, S. E. Storck, J. Rustenhoven, Z. Papadopoulos, T. Dykstra, F. Zhong, K. Kim, S. Blackburn, T. Mamuladze, O. Harari, C. M. Karch, R. J. Bateman, R. Perrin, M. Farlow, J. Chhatwal, Network Dominantly Inherited Alzheimer, S. Hu, G. J. Randolph, I. Smirnov, and J. Kipnis. 2022. 'Parenchymal border macrophages regulate the flow dynamics of the cerebrospinal fluid', *Nature*, 611: 585-93.

Earley, A. M., C. L. Graves, and C. E. Shiau. 2018. 'Critical Role for a Subset of Intestinal Macrophages in Shaping Gut Microbiota in Adult Zebrafish', *Cell Rep*, 25: 424-36.

Ellett, F., L. Pase, J. W. Hayman, A. Andrianopoulos, and G. J. Lieschke. 2010. 'mpeg1 promoter transgenes direct macrophage-lineage expression in zebrafish', *Blood*, 117: e49-56.

Ferrero, G., E. Gomez, S. Lyer, M. Rovira, M. Miserocchi, D. M. Langenau, J. Y. Bertrand, and V. Wittamer. 2020. 'The macrophage-expressed gene (mpeg) 1 identifies a subpopulation of B cells in the adult zebrafish', *J Leukoc Biol*, 107: 431-43.

Ferrero, G., C. B. Mahony, E. Dupuis, L. Yvernogeau, E. Di Ruggiero, M. Miserocchi, M. Caron, C. Robin, D. Traver, J. Y. Bertrand, and V. Wittamer. 2018. 'Embryonic Microglia Derive from Primitive Macrophages and Are Replaced by cmyb-Dependent Definitive Microglia in Zebrafish', *Cell Rep*, 24: 130-41.

Ferrero, G., M. Miserocchi, E. Di Ruggiero, and V. Wittamer. 2021. 'A csf1rb mutation uncouples two waves of microglia development in zebrafish', *Development*.

Franzen, O., L. M. Gan, and J. L. M. Bjorkegren. 2019. 'PanglaoDB: a web server for exploration of mouse and human single-cell RNA sequencing data', *Database (Oxford)*, 2019.

Gerrits, E., Y. Heng, Ewgm Boddeke, and B. J. L. Eggen. 2020. 'Transcriptional profiling of microglia; current state of the art and future perspectives', *Glia*, 68: 740-55.

Hammond, T. R., C. Dufort, L. Dissing-Olesen, S. Giera, A. Young, A. Wysoker, A. J. Walker, F. Gergits, M. Segel, J. Nemesh, S. E. Marsh, A. Saunders, E. Macosko, F. Ginhoux, J. Chen, R. J. M. Franklin, X.

826 Piao, S. A. McCarroll, and B. Stevens. 2018. 'Single-Cell RNA Sequencing of Microglia throughout
827 the Mouse Lifespan and in the Injured Brain Reveals Complex Cell-State Changes', *Immunity*.
828 Hason, M., T. Mikulasova, O. Machonova, A. Pombinho, T. J. van Ham, U. Irion, C. Nusslein-Volhard, P.
829 Bartunek, and O. Svoboda. 2022. 'M-CSFR/CSF1R signaling regulates myeloid fates in zebrafish via
830 distinct action of its receptors and ligands', *Blood Adv*, 6: 1474-88.
831 Herbomel, P., B. Thisse, and C. Thisse. 2001. 'Zebrafish early macrophages colonize cephalic mesenchyme
832 and developing brain, retina, and epidermis through a M-CSF receptor-dependent invasive
833 process', *Dev Biol*, 238: 274-88.
834 Hernández, P. P.; Strzelecka, P. M.; Athanasiadis, E. I.; Dominic Hall. D.; Robalo. A. F.; Collins, C. M.;
835 Boudinot, P.; Levraud, J. P.; Cvejic, A. 2018. 'Single-cell transcriptional analysis reveals ILC-like cells
836 in zebrafish', *Sci. Immunol.*, 3.
837 Jordao, M. J. C., R. Sankowski, S. M. Brendecke, Sagar, G. Locatelli, Y. H. Tai, T. L. Tay, E. Schramm, S.
838 Armbruster, N. Hagemeyer, O. Gross, D. Mai, O. Cicek, T. Falk, M. Kerschensteiner, D. Grun, and
839 M. Prinz. 2019. 'Single-cell profiling identifies myeloid cell subsets with distinct fates during
840 neuroinflammation', *Science*, 363.
841 Jurga, A. M., M. Paleczna, and K. Z. Kuter. 2020. 'Overview of General and Discriminating Markers of
842 Differential Microglia Phenotypes', *Front Cell Neurosci*, 14: 198.
843 Kaunzner, U. W., M. M. Miller, A. Gottfried-Blackmore, J. Gal-Toth, J. C. Felger, B. S. McEwen, and K.
844 Bulloch. 2012. 'Accumulation of resident and peripheral dendritic cells in the aging CNS', *Neurobiol*
845 *Aging*, 33: 681-93 e1.
846 Kuil, L. E., N. Oosterhof, G. Ferrero, T. Mikulasova, M. Hason, J. Dekker, M. Rovira, H. C. van der Linde, P.
847 M. van Strien, E. de Pater, G. Schaaf, E. M. Bindels, V. Wittamer, and T. J. van Ham. 2020. 'Zebrafish
848 macrophage developmental arrest underlies depletion of microglia and reveals Csf1r-
849 independent metaphocytes', *Elife*, 9.
850 Kuil, L. E., N. Oosterhof, S. N. Geurts, H. C. van der Linde, E. Meijering, and T. J. van Ham. 2019. 'Reverse
851 genetic screen reveals that Il34 facilitates yolk sac macrophage distribution and seeding of the
852 brain', *Dis Model Mech*, 12.
853 Langenau, D. M., A. A. Ferrando, D. Traver, J. L. Kutok, J. P. Hezel, J. P. Kanki, L. I. Zon, A. T. Look, and N. S.
854 Trede. 2004. 'In vivo tracking of T cell development, ablation, and engraftment in transgenic
855 zebrafish', *Proc Natl Acad Sci U S A*, 101: 7369-74.
856 Lewis, K. L., N. Del Cid, and D. Traver. 2014. 'Perspectives on antigen presenting cells in zebrafish', *Dev*
857 *Comp Immunol*, 46: 63-73.
858 Liu, Y. 2023. 'Zebrafish as a Model Organism for Studying Pathologic Mechanisms of Neurodegenerative
859 Diseases and other Neural Disorders', *Cell Mol Neurobiol*, 43: 2603-20.
860 Love, M. I., W. Huber, and S. Anders. 2014. 'Moderated estimation of fold change and dispersion for RNA-
861 seq data with DESeq2', *Genome Biol*, 15: 550.
862 Ludewig, P., M. Gallizioli, X. Urra, S. Behr, V. H. Brait, M. Gelderblom, T. Magnus, and A. M. Planas. 2016.
863 'Dendritic cells in brain diseases', *Biochim Biophys Acta*, 1862: 352-67.
864 Lugo-Villarino, G., K. M. Balla, D. L. Stachura, K. Banuelos, M. B. Werneck, and D. Traver. 2010.
865 'Identification of dendritic antigen-presenting cells in the zebrafish', *Proc Natl Acad Sci U S A*, 107:
866 15850-5.
867 Maddaluno, L., S. E. Verbrugge, C. Martinoli, G. Matteoli, A. Chiavelli, Y. Zeng, E. D. Williams, M. Rescigno,
868 and U. Cavallaro. 2009. 'The adhesion molecule L1 regulates transendothelial migration and
869 trafficking of dendritic cells', *J Exp Med*, 206: 623-35.
870 Masuda, T., R. Sankowski, O. Staszewski, C. Bottcher, L. Amann, C. Scheiwe, S. Nessler, P. Kunz, G. van Loo,
871 V. A. Coenen, P. C. Reinacher, A. Michel, U. Sure, R. Gold, J. Priller, C. Stadelmann, and M. Prinz.
872 2019. 'Spatial and temporal heterogeneity of mouse and human microglia at single-cell
873 resolution', *Nature*, 566: 388-92.

874 Masuda, Takahiro, Roman Sankowski, Ori Staszewski, and Marco Prinz. 2020. 'Microglia Heterogeneity in
875 the Single-Cell Era', *Cell Reports*, 30: 1271-81.
876 Mathias, J. R., K. B. Walters, and A. Huttenlocher. 2009. 'Neutrophil motility in vivo using zebrafish',
877 *Methods Mol Biol*, 571: 151-66.
878 Mazzolini, J., S. Le Clerc, G. Morisse, C. Coulonges, L. E. Kuil, T. J. van Ham, J. F. Zagury, and D. Sieger. 2019.
879 'Gene expression profiling reveals a conserved microglia signature in larval zebrafish', *Glia*.
880 Milner, J. J., C. Toma, B. Yu, K. Zhang, K. Omilusik, A. T. Phan, D. Wang, A. J. Getzler, T. Nguyen, S. Crotty,
881 W. Wang, M. E. Pipkin, and A. W. Goldrath. 2017. 'Runx3 programs CD8(+) T cell residency in non-
882 lymphoid tissues and tumours', *Nature*, 552: 253-57.
883 Minhas, Paras S., Amira Latif-Hernandez, Melanie R. McReynolds, Aarooran S. Durairaj, Qian Wang,
884 Amanda Rubin, Amit U. Joshi, Joy Q. He, Esha Gauba, Ling Liu, Congcong Wang, Miles Linde, Yuki
885 Sugiura, Peter K. Moon, Ravi Majeti, Makoto Suematsu, Daria Mochly-Rosen, Irving L. Weissman,
886 Frank M. Longo, Joshua D. Rabinowitz, and Katrin I. Andreasson. 2021. 'Restoring metabolism of
887 myeloid cells reverses cognitive decline in ageing', *Nature*.
888 Moore, F. E., E. G. Garcia, R. Lobbardi, E. Jain, Q. Tang, J. C. Moore, M. Cortes, A. Molodtsov, M. Kasheta,
889 C. C. Luo, A. J. Garcia, R. Mylvaganam, J. A. Yoder, J. S. Blackburn, R. I. Sadreyev, C. J. Ceol, T. E.
890 North, and D. M. Langenau. 2016. 'Single-cell transcriptional analysis of normal, aberrant, and
891 malignant hematopoiesis in zebrafish', *J Exp Med*, 213: 979-92.
892 Moyse, B. R., and R. J. Richardson. 2020. 'A Population of Injury-Responsive Lymphoid Cells Expresses
893 mpeg1.1 in the Adult Zebrafish Heart', *Immunohorizons*, 4: 464-74.
894 Mrdjen, D., A. Pavlovic, F. J. Hartmann, B. Schreiner, S. G. Utz, B. P. Leung, I. Lelios, F. L. Heppner, J. Kipnis,
895 D. Merkler, M. Greter, and B. Becher. 2018. 'High-Dimensional Single-Cell Mapping of Central
896 Nervous System Immune Cells Reveals Distinct Myeloid Subsets in Health, Aging, and Disease',
897 *Immunity*, 48: 380-95 e6.
898 Mundt, S., M. Greter, A. Flugel, and B. Becher. 2019. 'The CNS Immune Landscape from the Viewpoint of
899 a T Cell', *Trends Neurosci*, 42: 667-79.
900 Oosterhof, N., L. E. Kuil, H. C. van der Linde, S. M. Burm, W. Berdowski, W. F. J. van Ijcken, J. C. van Swieten,
901 E. M. Hol, M. H. G. Verheijen, and T. J. van Ham. 2018. 'Colony-Stimulating Factor 1 Receptor
902 (CSF1R) Regulates Microglia Density and Distribution, but Not Microglia Differentiation In Vivo',
903 *Cell Rep*, 24: 1203-17 e6.
904 Page, D. M., V. Wittamer, J. Y. Bertrand, K. L. Lewis, D. N. Pratt, N. Delgado, S. E. Schale, C. McGue, B. H.
905 Jacobsen, A. Doty, Y. Pao, H. Yang, N. C. Chi, B. G. Magor, and D. Traver. 2013. 'An evolutionarily
906 conserved program of B-cell development and activation in zebrafish', *Blood*, 122: e1-11.
907 Parichy DM, Ransom DG, Paw B, Zon LI, Johnson SL. 2000. 'An orthologue of the kit-related gene fms is
908 required for development of neural crest-derived xanthophores and a subpopulation of adult
909 melanocytes in the zebrafish, Danio rerio.', *Development*, 127: 3031-44.
910 Pasciuto, E., O. T. Burton, C. P. Roca, V. Lagou, W. D. Rajan, T. Theys, R. Mancuso, R. Y. Tito, L. Kouser, Z.
911 Callaerts-Vegh, A. G. de la Fuente, T. Prezzemolo, L. G. Mascali, A. Brajic, C. E. Whyte, L. Yshii, A.
912 Martinez-Muriana, M. Naughton, A. Young, A. Moudra, P. Lemaitre, S. Poovathingal, J. Raes, B. De
913 Strooper, D. C. Fitzgerald, J. Dooley, and A. Liston. 2020. 'Microglia Require CD4 T Cells to
914 Complete the Fetal-to-Adult Transition', *Cell*, 182: 625-40 e24.
915 Peri, F., and C. Nusslein-Volhard. 2008. 'Live imaging of neuronal degradation by microglia reveals a role
916 for v0-ATPase a1 in phagosomal fusion in vivo', *Cell*, 133: 916-27.
917 Raudvere, U., L. Kolberg, I. Kuzmin, T. Arak, P. Adler, H. Peterson, and J. Vilo. 2019. 'g:Profiler: a web server
918 for functional enrichment analysis and conversions of gene lists (2019 update)', *Nucleic Acids Res*,
919 47: W191-W98.

920 Rovira, M., M. Miserocchi, A. Montanari, L. Hammou, L. Chomette, J. Pozo, V. Imbault, X. Bisteau, and V.
921 Wittamer. 2022. 'Zebrafish Galectin 3 binding protein is the target antigen of the microglial 4C4
922 monoclonal antibody', *Dev Dyn*.
923 Satija, R., J. A. Farrell, D. Gennert, A. F. Schier, and A. Regev. 2015. 'Spatial reconstruction of single-cell
924 gene expression data', *Nat Biotechnol*, 33: 495-502.
925 Shiau, C. E., Z. Kaufman, A. M. Meireles, and W. S. Talbot. 2015. 'Differential requirement for irf8 in
926 formation of embryonic and adult macrophages in zebrafish', *PLoS One*, 10: e0117513.
927 Sieger, D., C. Moritz, T. Ziegenhals, S. Prykhozhij, and F. Peri. 2012. 'Long-range Ca2+ waves transmit brain-
928 damage signals to microglia', *Dev Cell*, 22: 1138-48.
929 Silva, N. J., L. C. Dorman, I. D. Vainchtein, N. C. Horneck, and A. V. Molofsky. 2021. 'In situ and
930 transcriptomic identification of microglia in synapse-rich regions of the developing zebrafish
931 brain', *Nat Commun*, 12: 5916.
932 Speirs, Z. C., C. A. Loynes, H. Mathiessen, P. M. Elks, S. A. Renshaw, and L. V. G. Jorgensen. 2024. 'What
933 can we learn about fish neutrophil and macrophage response to immune challenge from studies
934 in zebrafish', *Fish Shellfish Immunol*, 148: 109490.
935 Spits, H., and T. Cupedo. 2012. 'Innate lymphoid cells: emerging insights in development, lineage
936 relationships, and function', *Annu Rev Immunol*, 30: 647-75.
937 Stratoulias, V., J. L. Venero, M. E. Tremblay, and B. Joseph. 2019. 'Microglial subtypes: diversity within the
938 microglial community', *EMBO J*: e101997.
939 Talbot, J. C., and S. L. Amacher. 2014. 'A streamlined CRISPR pipeline to reliably generate zebrafish
940 frameshifting alleles', *Zebrafish*, 11: 583-5.
941 Tanabe, S., and T. Yamashita. 2018. 'B-1a lymphocytes promote oligodendrogenesis during brain
942 development', *Nat Neurosci*, 21: 506-16.
943 Tang, Q., N. S. Abdelfattah, J. S. Blackburn, J. C. Moore, S. A. Martinez, F. E. Moore, R. Lobbardi, I. M.
944 Tenente, M. S. Ignatius, J. N. Berman, R. S. Liwski, Y. Houvras, and D. M. Langenau. 2014.
945 'Optimized cell transplantation using adult rag2 mutant zebrafish', *Nat Methods*, 11: 821-4.
946 Tang, Q., S. Iyer, R. Lobbardi, J. C. Moore, H. Chen, C. Lareau, C. Hebert, M. L. Shaw, C. Neftel, M. L. Suva,
947 C. J. Ceol, A. Bernards, M. Aryee, L. Pinello, I. A. Drummond, and D. M. Langenau. 2017. 'Dissecting
948 hematopoietic and renal cell heterogeneity in adult zebrafish at single-cell resolution using RNA
949 sequencing', *J Exp Med*, 214: 2875-87.
950 Turrini, L., L. Roschi, G. de Vito, F. S. Pavone, and F. Vanzi. 2023. 'Imaging Approaches to Investigate
951 Pathophysiological Mechanisms of Brain Disease in Zebrafish', *Int J Mol Sci*, 24.
952 Van Hove, H., L. Martens, I. Scheyltjens, K. De Vlaminck, A. R. Pombo Antunes, S. De Prijck, N. Vandamme,
953 S. De Schepper, G. Van Isterdael, C. L. Scott, J. Aerts, G. Berx, G. E. Boeckxstaens, R. E.
954 Vandenbroucke, L. Vereecke, D. Moechars, M. Guilliams, J. A. Van Ginderachter, Y. Saeys, and K.
955 Movahedi. 2019. 'A single-cell atlas of mouse brain macrophages reveals unique transcriptional
956 identities shaped by ontogeny and tissue environment', *Nat Neurosci*, 22: 1021-35.
957 Vivier, E., D. Artis, M. Colonna, A. Diefenbach, J. P. Di Santo, G. Eberl, S. Koyasu, R. M. Locksley, A. N. J.
958 McKenzie, R. E. Mebius, F. Powrie, and H. Spits. 2018. 'Innate Lymphoid Cells: 10 Years On', *Cell*,
959 174: 1054-66.
960 Vivier, E., S. A. van de Pavert, M. D. Cooper, and G. T. Belz. 2016. 'The evolution of innate lymphoid cells',
961 *Nat Immunol*, 17: 790-4.
962 Wittamer, V., J. Y. Bertrand, P. W. Gutschow, and D. Traver. 2011. 'Characterization of the mononuclear
963 phagocyte system in zebrafish', *Blood*, 117: 7126-35.
964 Wong, S. H., J. A. Walker, H. E. Jolin, L. F. Drynan, E. Hams, A. Camelo, J. L. Barlow, D. R. Neill, V. Panova,
965 U. Koch, F. Radtke, C. S. Hardman, Y. Y. Hwang, P. G. Fallon, and A. N. McKenzie. 2012.
966 'Transcription factor RORalpha is critical for nuocyte development', *Nat Immunol*, 13: 229-36.

967 Wu, S. , L. T. M. Nguyen, H. Pan, S. Hassan, Y. Dai, J. Xu, and Z. Wen. 2020. 'Two phenotypically and
968 functionally distinct microglial populations in adult zebrafish', *Science Advances*.
969 Wu, S. Y., J. Shin, D. S. Sepich, and L. Solnica-Krezel. 2012. 'Chemokine GPCR signaling inhibits beta-catenin
970 during zebrafish axis formation', *PLoS Biol*, 10: e1001403.
971 Xie, Z., A. Bailey, M. V. Kuleshov, D. J. B. Clarke, J. E. Evangelista, S. L. Jenkins, A. Lachmann, M. L.
972 Wojciechowicz, E. Kropiwnicki, K. M. Jagodnik, M. Jeon, and A. Ma'ayan. 2021. 'Gene Set
973 Knowledge Discovery with Enrichr', *Curr Protoc*, 1: e90.
974 Xu, H., T. Xiao, C. H. Chen, W. Li, C. A. Meyer, Q. Wu, D. Wu, L. Cong, F. Zhang, J. S. Liu, M. Brown, and X.
975 S. Liu. 2015. 'Sequence determinants of improved CRISPR sgRNA design', *Genome Res*, 25: 1147-
976 57.
977 Yanez, A., and H. S. Goodridge. 2016. 'Interferon regulatory factor 8 and the regulation of neutrophil,
978 monocyte, and dendritic cell production', *Curr Opin Hematol*, 23: 11-7.
979 Yoder, J. A., P. M. Turner, P. D. Wright, V. Wittamer, J. Y. Bertrand, D. Traver, and G. W. Litman. 2010.
980 'Developmental and tissue-specific expression of NITRs', *Immunogenetics*, 62: 117-22.
981 Zhou, Q., C. Zhao, Z. Yang, R. Qu, Y. Li, Y. Fan, J. Tang, T. Xie, and Z. Wen. 2023. 'Cross-organ single-cell
982 transcriptome profiling reveals macrophage and dendritic cell heterogeneity in zebrafish', *Cell*
983 *Rep*, 42: 112793.

984

Reagent type (species) or resource	Designation	Source or reference	Identifiers	Additional information
Genetic reagent (*Danio rerio*)	*Tg(mhc2dab:GFP$_{LT}$)^{sd67}*	(Wittamer et al. 2011)	ZFIN: *sd67*	
Genetic reagent (*Danio rerio*)	*Tg(ptprc:DsRed^{express})^{sd3}*	(Wittamer et al. 2011)	ZFIN: *sd3*	
Genetic reagent (*Danio rerio*)	*Tg(mpeg1.1:eGFP)^{gl22}*	(Ellett et al. 2010)	ZFIN: *gl22*	
Genetic reagent (*Danio rerio*)	*Tg(mpeg1.1:mCherry)^{gl23}*	(Ellett et al. 2010)	ZFIN: *gl23*	
Genetic reagent (*Danio rerio*)	*TgBAC(p2ry12:p2ry12-GFP)^{hdb3}*	(Sieger et al. 2012)	ZFIN: *hdb3*	
Genetic reagent (*Danio rerio*)	*Tg(lck:lck-eGFP)^{cz1}*	(Langenau et al. 2004)	ZFIN: *cz1*	
Genetic reagent (*Danio rerio*)	*TgBAC(cd4-1:mcherry)^{UMC13}*	(Dee et al. 2016)	ZFIN: *UMC13*	
Genetic reagent (*Danio rerio*)	*Tg(Cau.Ighv-ighm:EGFP)^{sd19}*	(Page et al. 2013)	ZFIN: *sd19*	
Genetic reagent (*Danio rerio*)	*Tg(mpx:GFP)^{i113}*	(Mathias, Walters, and Huttenlocher 2009)	ZFIN: *i113*	
Genetic reagent (*Danio rerio*)	*panther^{j4e1}*	(Parichy DM 2000)	ZFIN: *i4e1*	
Genetic reagent (*Danio rerio*)	*csf1rb^{sa1503}*	Sanger Institute Zebrafish Mutation Project	ZFIN: *sa1503*	
Genetic reagent (*Danio rerio*)	*irf8^{std96}*	(Shiau et al. 2015)	ZFIN: *std96*	
Genetic reagent (*Danio rerio*)	*rag2^{E450fs}*	(Tang et al. 2014)	ZFIN: *E450fs*	
Genetic reagent (*Danio rerio*)	*batf3^{ulb31}*	This manuscript	ZFIN: *ulb31*	
Antibody	Anti-GFP (chicken polyclonal)	Abcam	RRID:AB_300798	1:500
Antibody	Anti-Lcp1 (rabbit)	In house		1:1000
Antibody	Anti-mCherry (mouse monoclonal)	Takara Bio	RRID:AB_2307319	1:500
Antibody	Alexa Fluor 488-conjugated anti-chicken IgG	Abcam	RRID:AB_2636803	1:500
Antibody	Alexa Fluor 594-conjugated anti-rabbit IgG	Abcam	RRID:AB_2782993	1:500

Antibody	Alexa Fluor 647-conjugated anti-mouse IgG	Abcam	RRID:AB_2890037	1:500
Commercial assay or kit	SP6 RNA Polymerase	New England BioLabs	Cat# M0207	
Commercial assay or kit	High Pure PCR Cleanup Microkit	Roche	Cat# 498395500	
Commercial assay or kit	Rneasy Plus mini kit	Qiagen	Cat# 74134	
Chemical compound, drug	SYTOX™Red	Invitrogen	Cat# S34859	
Chemical compound, drug	qScript cDNA SuperMix	Quanta Biosciences	Cat# 95048-100	
Software, algorithm	Flow-Jo LLC	TreeStar	RRID:SCR_008520	
Software, algorithm	Black Zen software	Zeiss, Germany	RRID:SCR_018163	
Software, algorithm	Blue Zen software	Zeiss, Germany	RRID:SCR_013672	
Software, algorithm	R Statistical software v. 4.0.3	R Project for Statistical Computing	RRID:SCR_001905	
Software, algorithm	GraphPad Prism 8	GraphPad software, USA	RRID:SCR_002798	

985

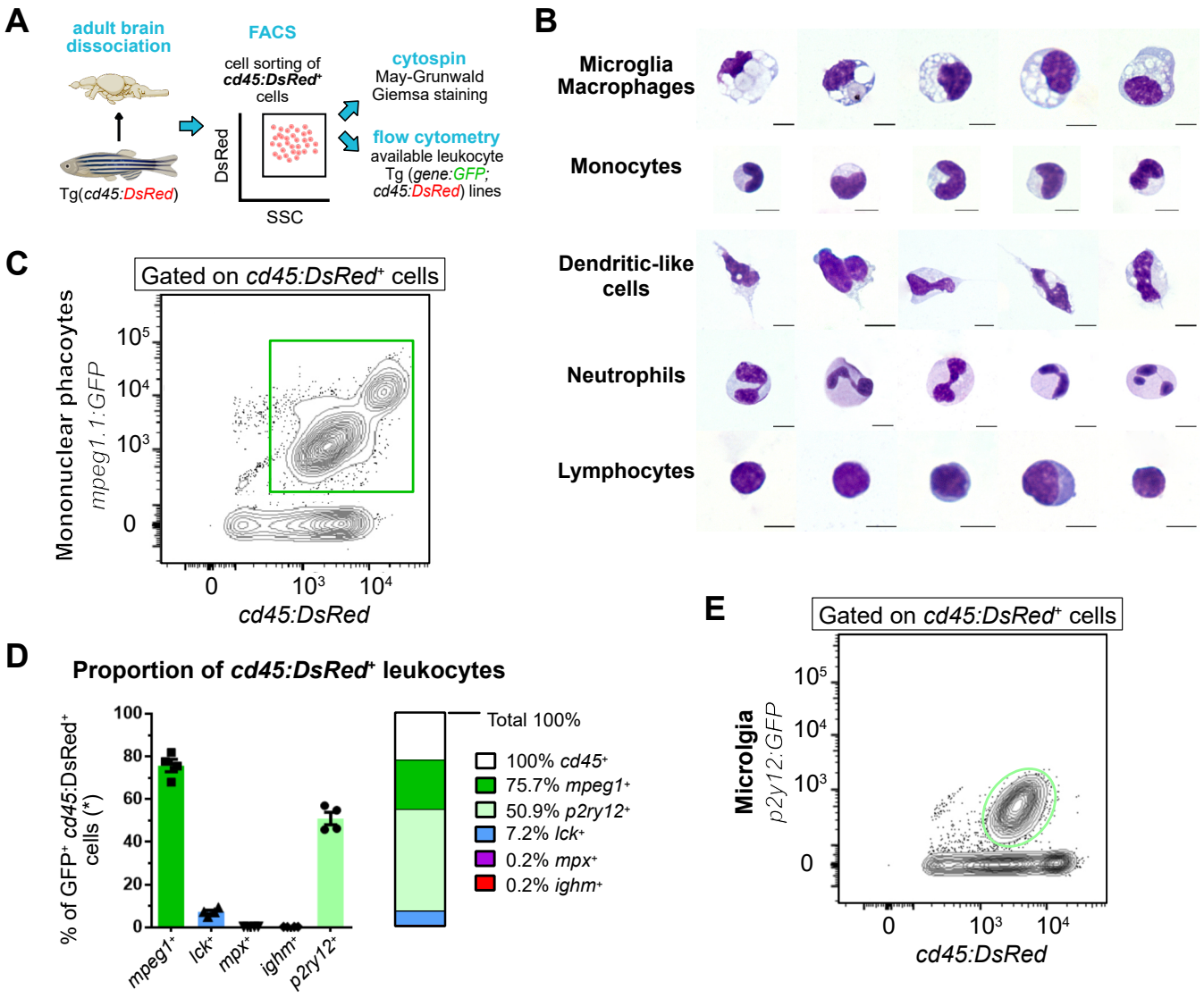

Figure 1. Leukocyte heterogeneity in the adult zebrafish brain using blood lineage-specific transgenic lines. **A.** Schematic overview of the experiment. First, *cd45:DsRed*$^+$ cells were sorted, cytospined and stained with May-Grunwald Giemsa (MGG). In parallel, lines carrying the *cd45*:DsRed transgene in combination with blood lineage-specific GFP reporters were analyzed by flow cytometry. **B.** Morphology of brain-sorted *cd45:DsRed*$^+$ cells stained with MGG. Microglia and/or macrophages, monocytes, dendritic cells, neutrophils and lymphocytes were identified. The scale bar represents 5 µm. **C.** Flow cytometry analysis on brain cell suspensions from adult *Tg(mpeg1:GFP; cd45:DsRed)* identifying *mpeg1:GFP*$^+$*; cd45:DsRed*$^+$ mononuclear phagocytes (green gate). **D.** Proportion of brain immune cell types, as determined by flow cytometry analysis on cell suspensions from fish carrying *cd45:DsRed*$^+$ and a lineage-specific GFP reporter (*n*=4 fish). The percentage relative to total *cd45:DsRed*$^+$ leukocytes is shown, with the exception of *Tg(ighm:GFP; cd45:DsRed)* which are not normalized as the *cd45:DsRed* transgene is not expressed in the B cell lineage. **E.** Flow cytometry analysis of brain cell suspensions from an adult *Tg(p2ry12:p2ry12-GFP; cd45:DsRed)* fish, identifying *p2ry12:p2ry12-GFP*$^+$*; cd45:DsRed*$^+$ microglial cells (light green gate). *n* refers to the number of biological replicates. Data in (D) are mean ± SEM.

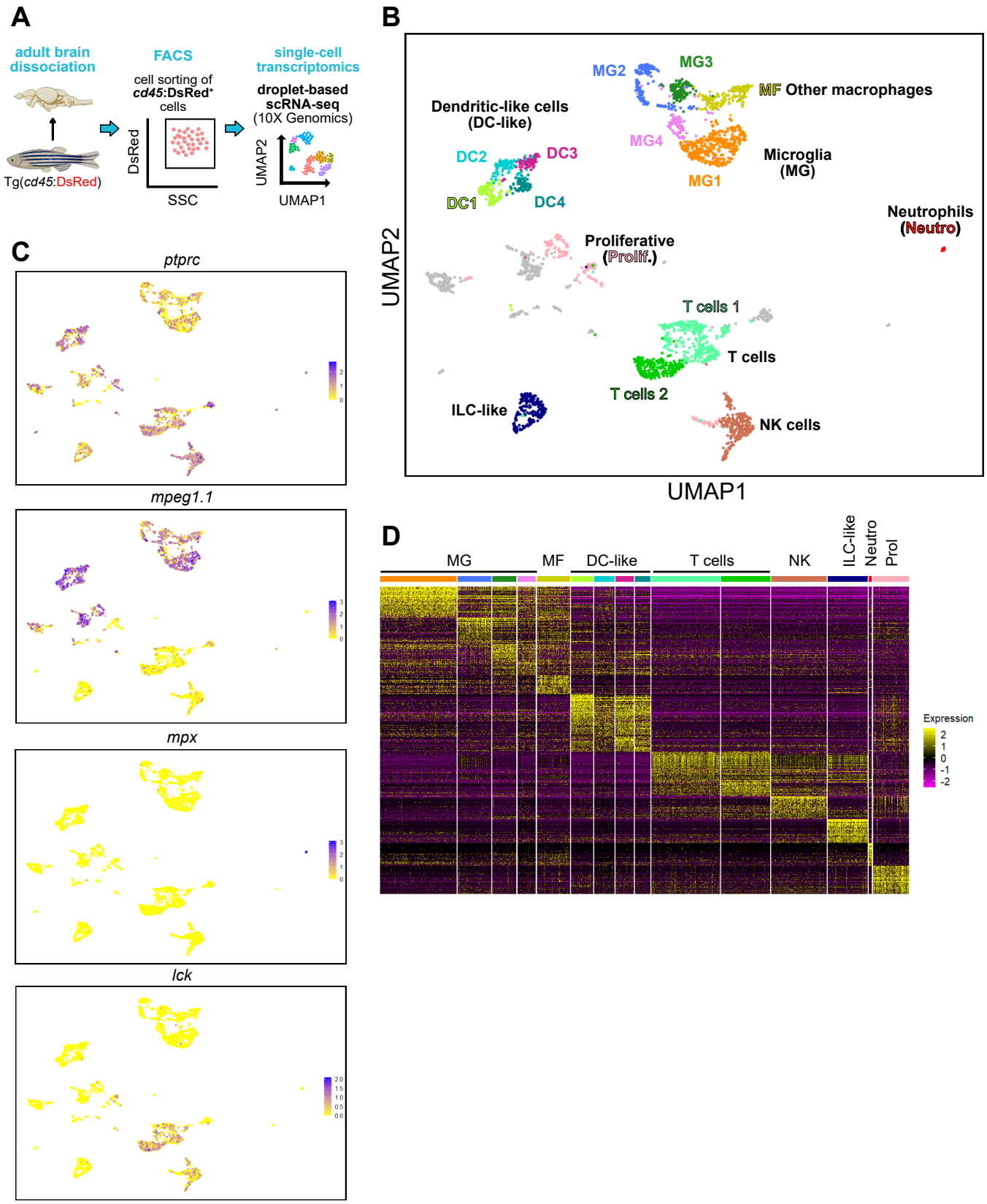

Figure 2. Diversity of brain leukocytes as shown by single-cell transcriptomics. A. Schematic overview of the experimental approach. Single-cell profiling of total brain *cd45:DsRed*$^{+}$ leukocytes (pool from 3 individual fish) was performed using the 10X Genomics platform. **B.** Split Uniform Manifold Approximation Projection (UMAP) of brain *cd45:DsRed*$^{+}$ cells with annotated cell populations. Clusters in grey shade are not indicative of a specific cell type and were not annotated. **C.** UMAP plots depicting the expression pattern of *ptprc*, also known as *cd45* (leukocytes), *mpeg1.1* (mononuclear phagocytes), *mpx* (neutrophils) and *lck* (T and NK lymphocytes). Gene expression levels from low to high are indicated by a color gradient from yellow to purple (normalized counts in log1p). **D.** Heat map of the top differentially up-regulated genes in each cluster (row=gene, column=cell type). Color scale (gradual from purple to yellow) indicates the expression level (average $\log_2$ fold change).

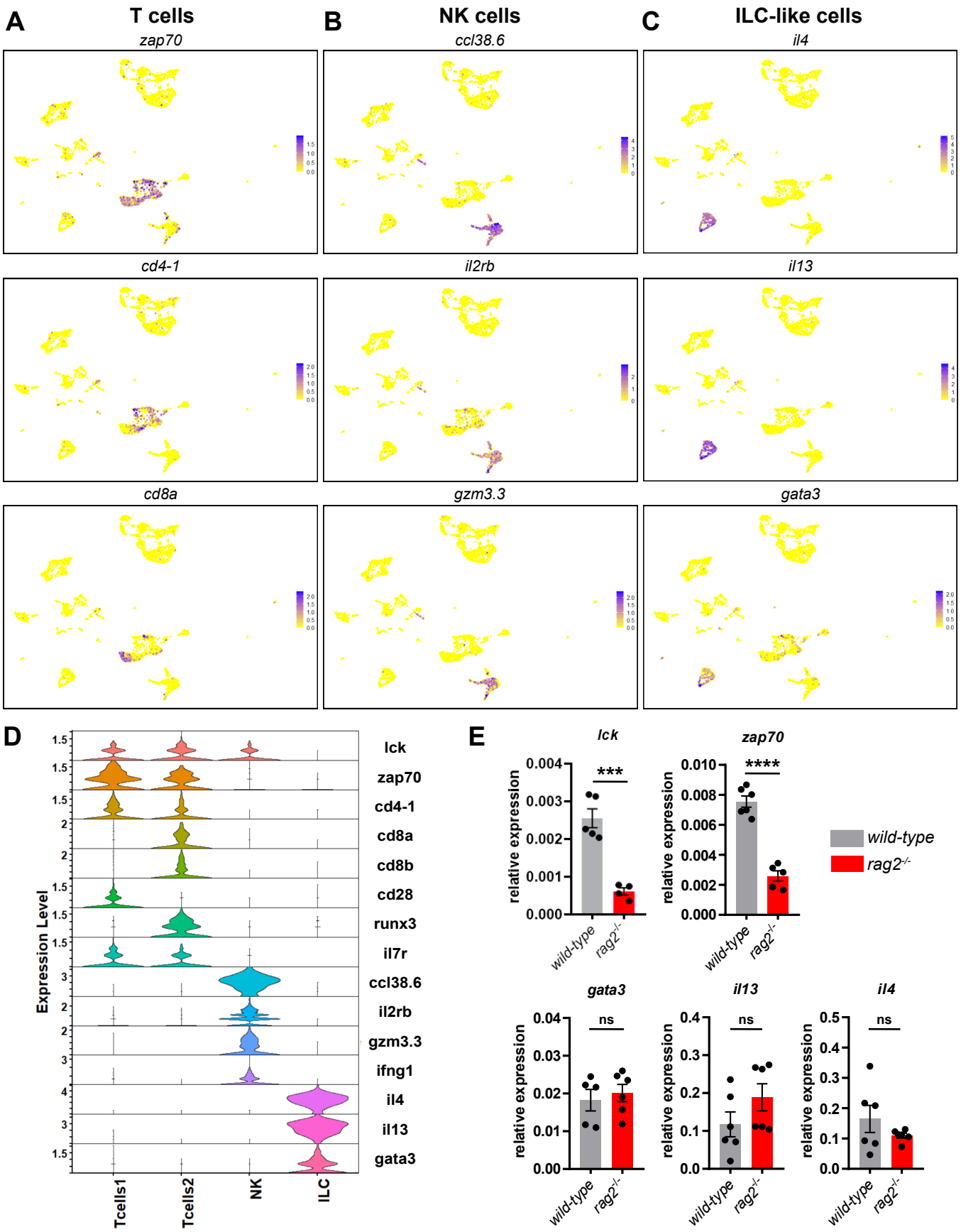

Figure 3. Single-cell RNA sequencing identifies several lymphocyte subpopulations in the adult brain. A-C. UMAP visualization of the expression of selected genes in the annotated T cell clusters Tcells1 and Tcells2 (*zap70*, *cd4-1* and *cd8a*), NK cluster (*ccl38.6*, *il2rb*, *gzm3.3*) and ILC-like cluster (*il4*, *il13* and *gata3*). Color scale (gradual from yellow to purple) indicates the expression level for each gene (normalized counts in log1p). **D.** Violin plots representing the expression levels of known lymphocyte markers (normalized counts in log1p) within the different clusters. **E.** Comparison of the relative expression of *lck*, *zap70*, *gata3*, *il13* and *il4* transcripts between brain *cd45:DsRed*$^{+}$ cells isolated by FACS from T cell-deficient *rag2*$^{-/-}$ mutants (red bars) and their *wild-type* siblings (grey bars). Each data point represents an individual fish (n=6) and error bars indicate SEM. *** P<0.001, **** P<0.0001 (Two-tailed unpaired t-test).

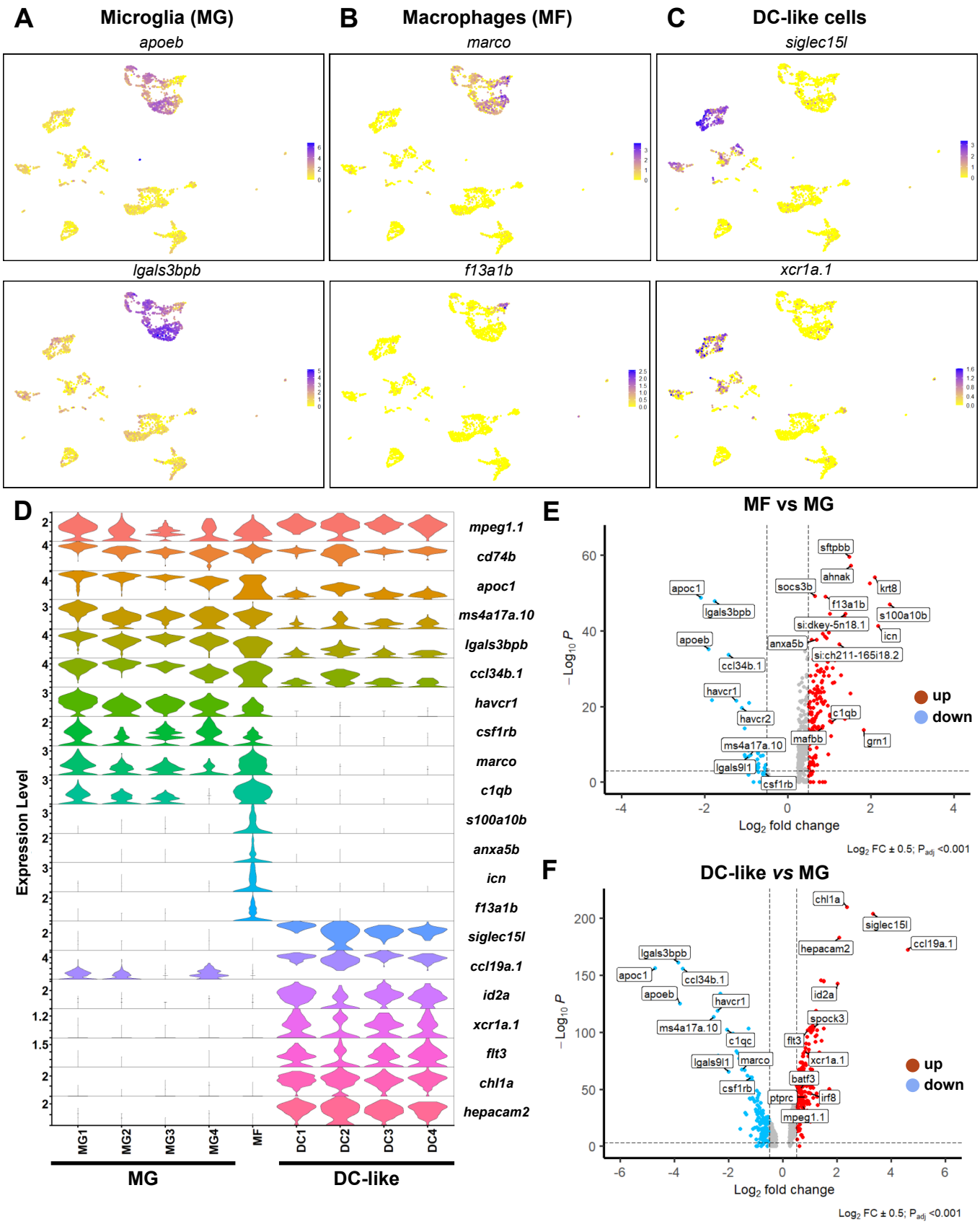

Figure 4. Heterogenous subsets of mononuclear phagocytes exist in the zebrafish brain. A-C. UMAP visualization of the expression of selected genes in the microglia (*apoeb* and *lgals3bpb*) (A), non-microglia macrophage (*marco* and *f13a1b*) (B) and DC-like (*xcr1a.1* and *siglec15l*) (C) cell clusters. Color scale (gradual from yellow to purple) indicates the expression level for each gene (normalized counts in log1p). **D.** Violin plot analysis comparing the expression levels of selected genes (y-axis, normalized counts in log1p) between the different mononuclear phagocyte cell clusters. **E.** Volcano plot showing the differentially expressed (DE) genes between microglia (MG) and non-microglia macrophages (MF). Lines indicate significantly DE genes ($\log_2$ fold-change >|0.5|, $-\log_{10}$ P_{adj} <0.001). Red dots represent up-regulated genes and blue dots down-regulated genes. Labels show representative DE genes identified in the analysis. **F.** Volcano plot showing the DE genes between microglia (MG) and DC-like cells (DC-like). Lines indicate significantly DE genes ($\log_2$ fold-change >|0.5|, $-\log_{10}$ P_{adj} <0.001).

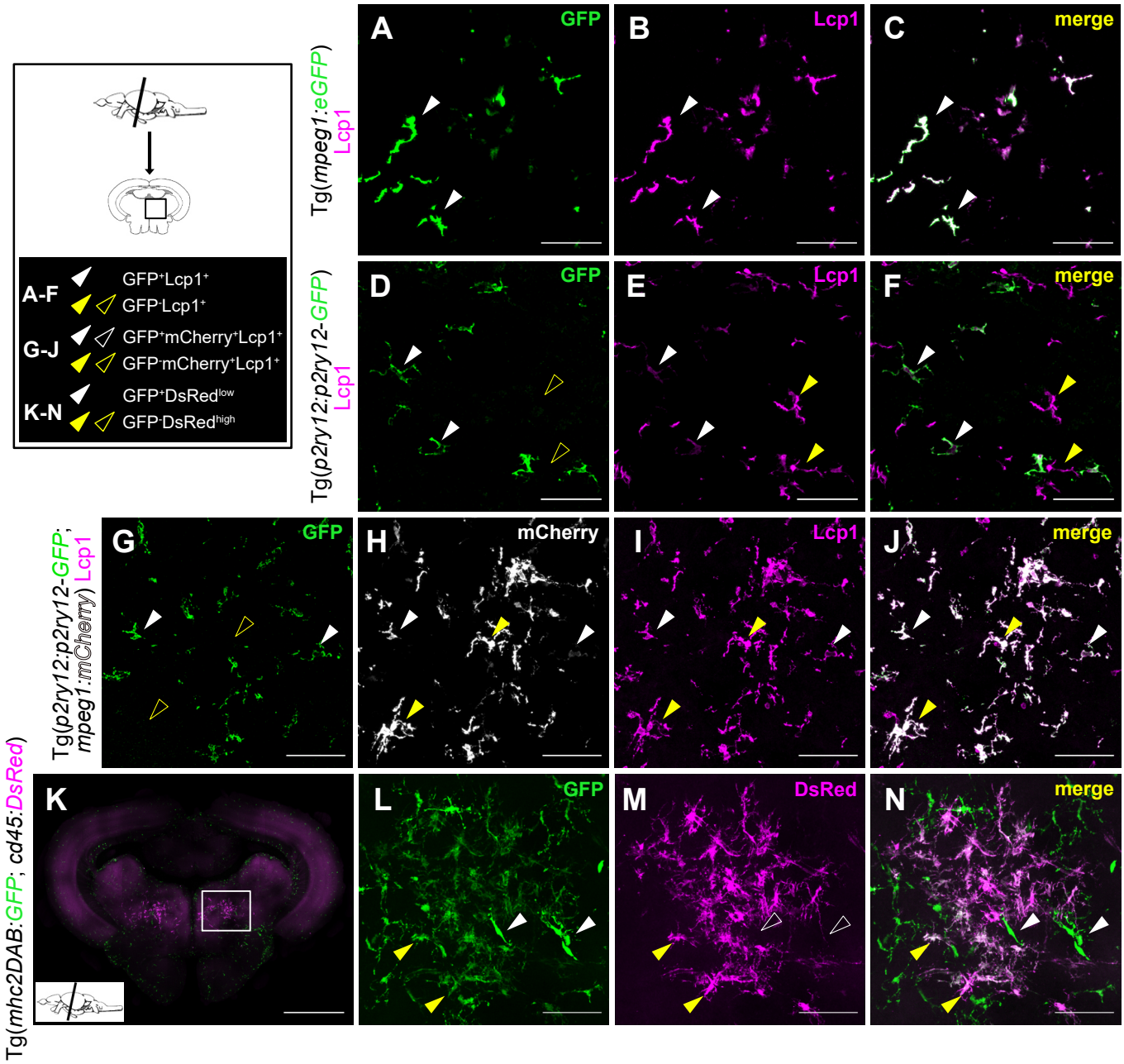

Figure 5. DC-like cells localize together with microglia within the brain parenchyma. A-F. Immunofluorescence on transversal brain sections (14 µm) from *Tg(mpeg1:GFP)* (A-C) or *Tg(p2ry12:p2ry12-GFP*) (D-F) transgenic adult fish co-immunostained with anti-GFP (green) and anti-Lcp1 (magenta) antibodies. **A-C.** All *mpeg1*:GFP$^+$ mononuclear phagocytes in the brain parenchyma display Lcp1 immunostaining, as expected. **D-F.** Similarly, all microglial cells, identified by GFP expression in the brain parenchyma of *Tg(pr2y12:p2ry12-GFP)* fish, are Lcp1$^+$, as expected. **G-J.** In sections of adult *Tg(p2ry12:p2ry12-GFP; mpeg1:mCherry)* double transgenic animals, GFP labeling is not observed in all mCherry$^+$ cells. GFP (green), mCherry (grey), Lcp1 (magenta) and merge of the three channels. All images were taken using a 20X objective and correspond to orthogonal projections. White arrowheads point to microglial cells (GFP$^+$; Lcp1$^+$or GFP$^+$; mCherry$^+$; Lcp1$^+$) and yellow arrowheads to DC-like cells (GFP$^-$; Lcp1$^+$ or GFP$^-$; mCherry$^+$; Lcp1$^+$). Scale bars: 50 µm. **K-N.** Confocal imaging of a midbrain vibratome section (100 µm) from an adult *Tg(mhc2dab:GFP; cd45:DsRed)* brain. GFP (green), DsRed (magenta) and merge of the two channels are shown. Images correspond to orthogonal projections, white arrowheads point to GFP$^+$; DsRed$^+$ cells and yellow arrowheads to GFP$^-$; DsRed^{high}. Scale bar in (K): 500 µm, scale bar in (L-N): 50 µm. Images are representative of brain tissue sections from 2-3 fish.

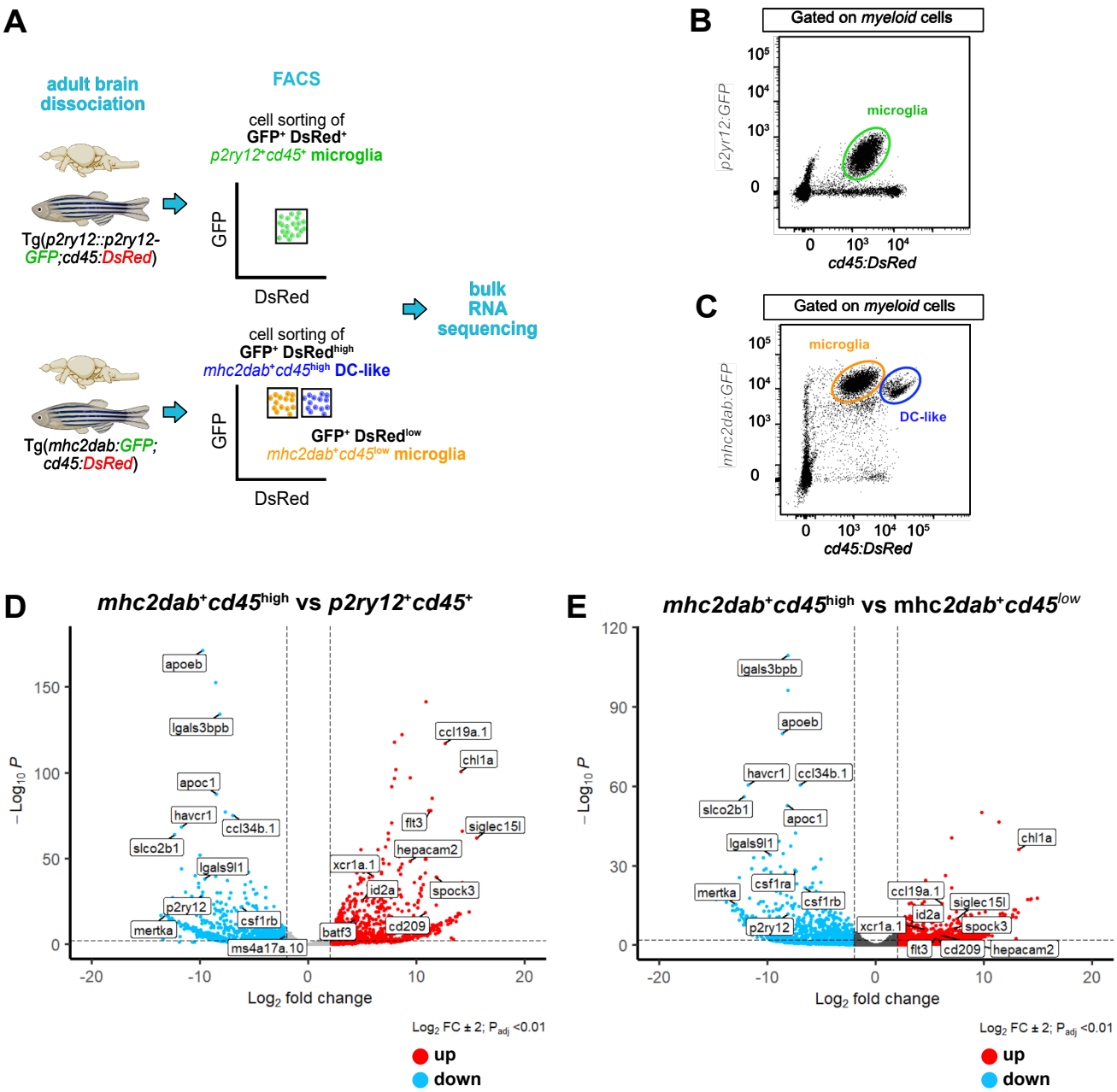

Figure 6. Transcriptomic analysis of microglia (*p2ry12⁺; cd45⁺* or *mhc2dab⁺; cd45^{low}*) and DC-like cells (*mhc2dab⁺; cd45^{high}*). A. Schematic overview of the experiments. Microglia were isolated using *Tg(p2ry12:p2ry12-GFP; cd45:DsRed)* or *Tg(mhc2dab:GFP; cd45:DsRed)* transgenic fish, and DC-like cells using the *Tg(mhc2dab:GFP; cd45:DsRed)* reporter line. **B.** Representative flow cytometry plot identifying microglial cells in brain cell suspensions from *Tg(p2ry12:p2ry12-GFP; cd45:DsRed)* fish. **C.** Representative flow cytometry plot identifying *mhc2dab:GFP⁺; cd45:DsRed^{low}* microglia from *mhc2dab:GFP⁺; cd45:DsRed^{high}* DC-like cells in brain cell suspensions from *Tg(mhc2dab:GFP; cd45:DsRed)* fish. **D.** Volcano plot showing the differentially expressed (DE) genes between *mhc2dab⁺; cd45^{high}* DC-like cells and *p2ry12⁺; cd45⁺* microglia. Red dots represent up-regulated genes and blue dots down-regulated genes. Lines indicate significantly DE genes ($\log_2$ fold-change >|2|, $-\log_{10}$ P_{adj} <0.01). Labels show marker genes for DC-like cells and microglia identified in the scRNA-sequencing analysis. **E.** Volcano plot showing the DE genes between *mhc2dab⁺; cd45^{high}* DC-like cells (blue) and *mhc2dab⁺cd45^{low}* microglia (red). Lines indicate significantly DE genes ($\log_2$ fold-change >|2|, $-\log_{10}$ P_{adj} <0.01).

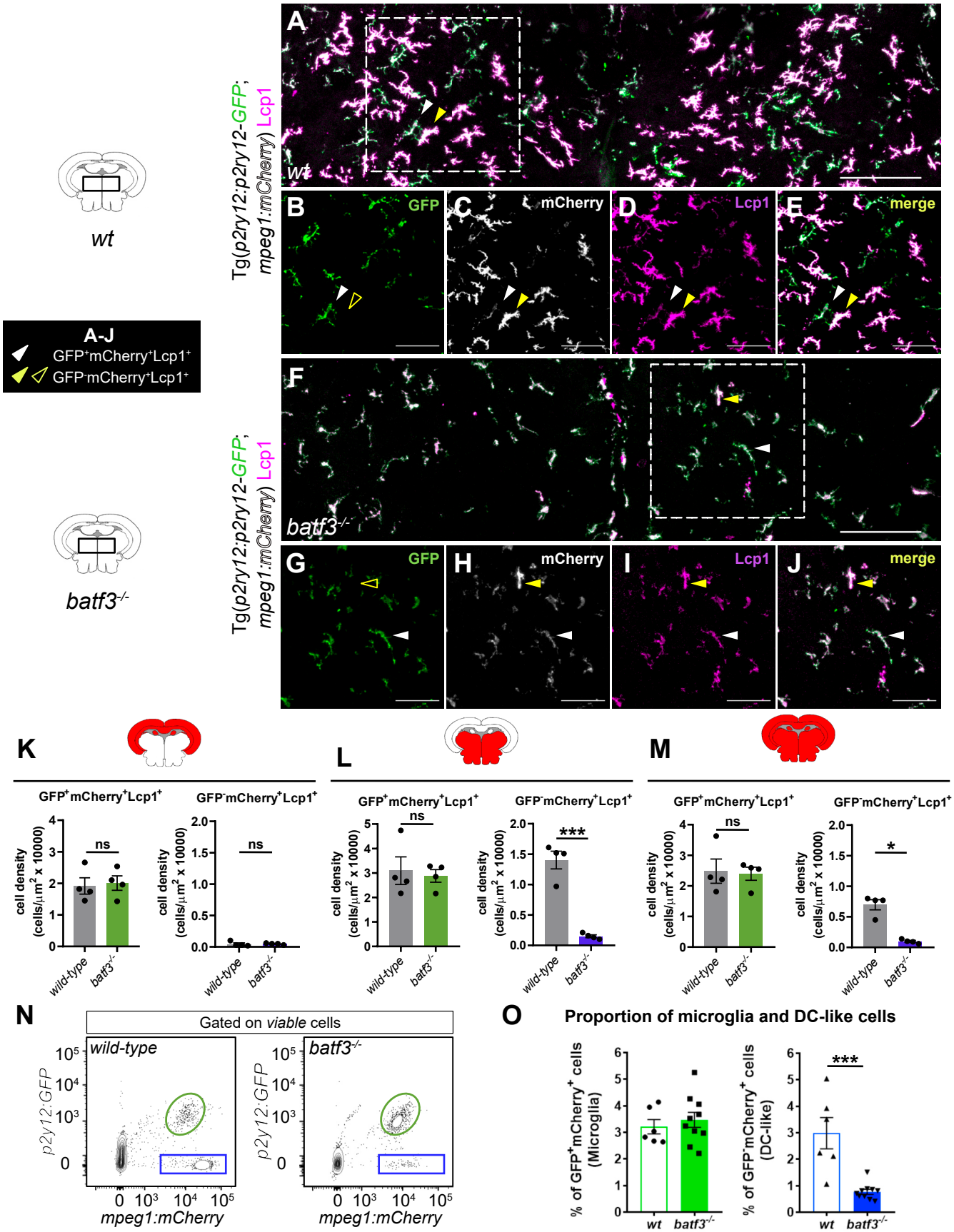

Figure 7. Brain DC-like cells are lost in *batf3*$^{-/-}$ mutant fish. A-J. Immunofluorescence on transverse brain sections (14 µm) from adult *wild-type* (A-E) and *batf3*$^{-/-}$ mutant (F-J) fish carrying the *Tg(p2ry12:p2ry12-GFP; mpeg1:mCherry)* double transgene and immunostained for GFP (green), mCherry (grey) and Lcp1 (magenta). Illustrative case of the merge of the three channels (A, F) allowing to identify GFP^{+}; mCherry^{+}; Lcp1^{+} microglia (white arrowheads) versus GFP^{-}; mCherry^{+}; Lcp1^{+} DC-like cells (yellow arrowheads). While DC-like cells are found in high numbers within the ventral part of control parenchyma (A), these are dramatically decreased following genetic loss of *batf3* (F). Scale bars: 100 µm. (B-E, G-J). Single channels high magnification of the insets in A (B-E) and F (G-J). Scale bars: 50 µm. Images were taken using a 20X objective and correspond to orthogonal projections. **K-M.** Quantification of cell density for GFP^{+}; mCherry^{+}; Lcp1^{+} microglia and GFP^{-}; mCherry^{+}; Lcp1^{+} DC-like cells in the dorsal midbrain area or optic tectum (K), ventral midbrain area (L) and the entire section (M) of control (grey bars) and *batf3*$^{-/-}$ (green bars) fish. Each dot

represents a single fish and data are mean ± SEM. * P<0.05 (Mann-Whitney test), *** P<0.0001 (Two-tailed unpaired t-test). **N.** Flow cytometry analysis of brain cell suspensions from *wild-type* and *batf3*$^{-/-}$ adult fish carrying the *Tg(p2ry12:p2ry12-GFP; mpeg1:mCherry)* reporter. The GFP^{+}; mCherry^{+} fraction identifies microglia (green circle), whereas the GFP^{-}; mCherry^{+} fraction contains mainly DC-like cells (blue frame). **O.** Percentage of microglia and DC-like cells in brain cell suspensions for each genotype, relative to the whole living brain population, as shown in (N) (*wild-type*, *n*=6; *batf3*$^{-/-}$, *n*=10). *** P<0.001 (Two-tailed unpaired t-test). *n* refers to number of biological replicates.

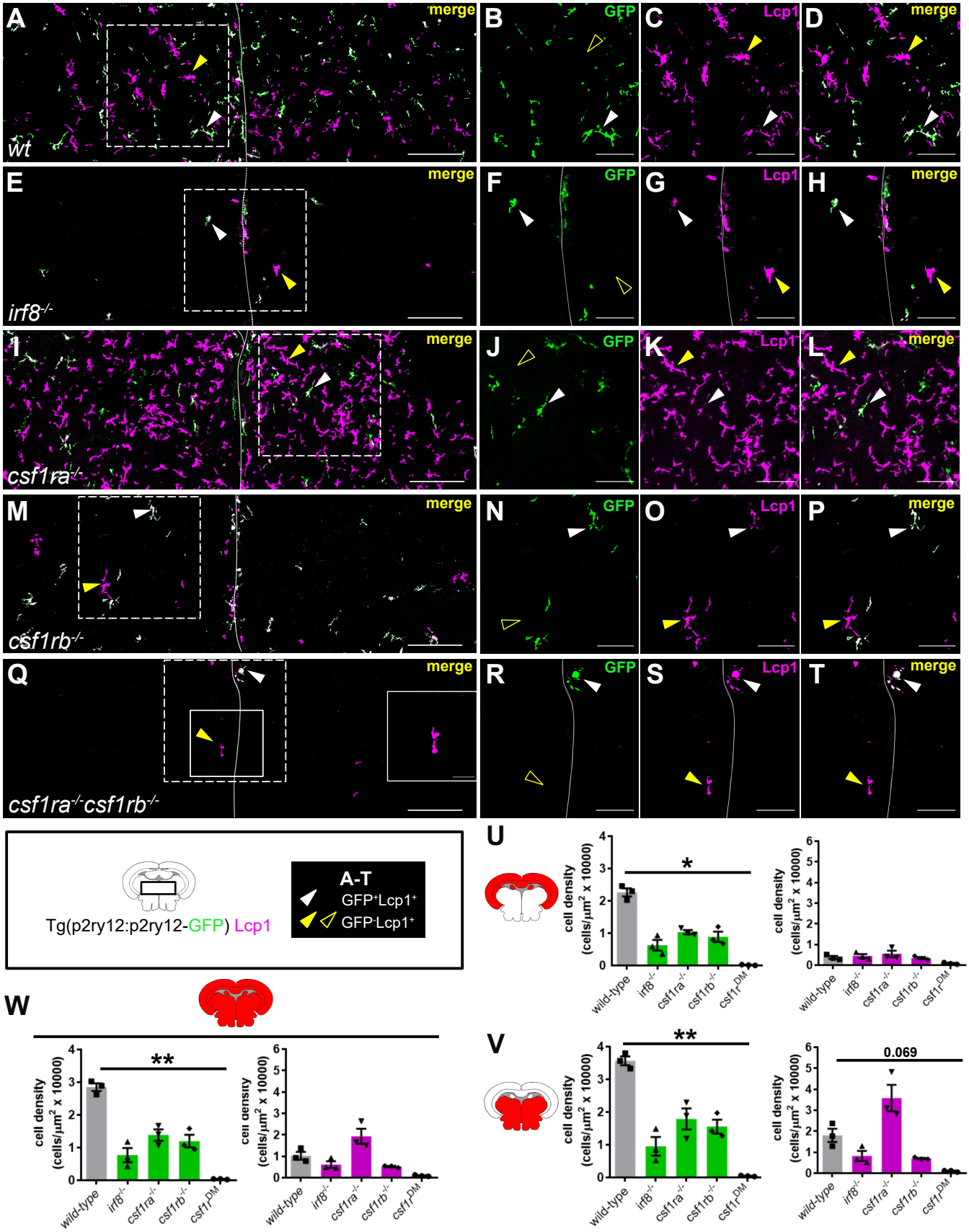

Figure 8. Examination of microglia and DC-like cells in myeloid–deficient mutant lines. A-D. Immunofluorescence on transverse brain sections from *Tg(p2ry12:p2ry12-GFP)* transgenic adult *wild-type* (A-D), *irf8*$^{-/-}$ (E-H), *csf1ra*$^{-/-}$ (I-L), *csf1rb*$^{-/-}$ (M-P) and *csf1ra*$^{-/-}$*; csf1rb*$^{-/-}$ *(csf1r*^{DM}*)* (Q-T) fish, co-stained with anti-GFP (green) and Lcp1 (magenta) antibodies. **A, E, I, M, Q.** For each genotype, illustrative case of the merge of the two channels , allowing to discriminate in the parenchyma GFP^{+}; Lcp1^{+} microglia (white arrowheads) from GFP^{-}; Lcp1^{+} DC-like cells (yellow arrowheads). Single channels high magnification of the insets (dashed frame) in A (B-D), E (F-H), I (J-L), M (N-P) and Q (R-T). Outline yellow arrowheads indicate the absence of GFP signal in corresponding yellow arrowhead pointed cells. Scale bar in (A), (E), (I), (M) and (Q) represents 100 µm and scale bar in other images 50 µm. **U-V.** Quantification of the cell density for GFP^{+}Lcp1^{+} microglia and GFP^{-}Lcp1^{+} DC-like cells in the dorsal (U), ventral (V) and whole area (W) of the brain for each genotype (*n*=3). Data in U-W are mean ± SEM. *P<0.05 , **P<0.01 (Klustal-Wallis test with Dunn's post-hoc).